Macrophage enzyme and reduced inflammation drive brain correction of mucopolysaccharidosis IIIB by stem cell gene therapy

Rebecca J Holley*, S M Ellison*, D Fil*, C O'Leary*, J McDermott*, N Senthivel*, A Langford-Smith*[$], F L Wilkinson*[$], Z D'Souza*, H Parker*, A Liao*, S Rowlston*, H Gleitz*, S-h Kan[#], P I Dickson[#] & B W Bigger*[+]

**Stem Cell and Neurotherapies, Faculty of Biology, Medicine and Health, University of Manchester, Manchester, UK*

[$]Vascular Pathology Group, Centre for Biomedicine, School of Healthcare Science, Faculty of Science and Engineering, Manchester Metropolitan University, John Dalton Building, Chester Street, Manchester, UK, M1 5GD

[#]Department of Paediatrics, Los Angeles Biomedical Research Institute at Harbor-UCLA, Torrance, CA, 90502, United States of America

[+]Corresponding author: Dr Brian Bigger, Stem Cell and Neurotherapies, Division of Cell Matrix Biology and Regenerative Medicine, Faculty of Biology, Medicine and Health, 3.721 Stopford Building, Oxford Road, University of Manchester, Manchester, M13 9PT. UK.

Running Title: Stem cell gene therapy for MPSIIIB

Abstract

Mucopolysaccharidosis IIIB is a paediatric lysosomal storage disease caused by deficiency of the enzyme α-*N*-acetylglucosaminidase (NAGLU), involved in the degradation of the glycosaminoglycan heparan sulphate. Absence of NAGLU leads to accumulation of partially degraded heparan sulphate within lysosomes and the extracellular matrix, giving rise to severe central nervous system degeneration with progressive cognitive impairment and behavioural problems. There are no therapies. Haematopoietic stem cell transplant shows great efficacy in the related disease mucopolysaccharidosis I, where donor-derived monocytes can transmigrate into the brain following bone marrow engraftment, secrete the missing enzyme and cross-correct neighbouring cells. However, little neurological correction is achieved in

mucopolysaccharidosis IIIB patients. We have therefore developed an *ex vivo* haematopoietic stem cell gene therapy approach in a mouse model of mucopolysaccharidosis IIIB, utilising a high-titre lentiviral vector and the myeloid-specific CD11b promoter, driving the expression of NAGLU (LV.NAGLU). In order to understand the mechanism of correction we also compared this with a poorly secreted version of NAGLU containing a C-terminal fusion to IGFII (LV.NAGLU-IGFII). Mucopolysaccharidosis IIIB haematopoietic stem cells were transduced with vector, transplanted into myeloablated mucopolysaccharidosis IIIB mice and compared at 8 months of age with mice receiving a wild-type transplant. As the disease is characterised by increased inflammation, we also tested the anti-inflammatory steroidal agent prednisolone alone, or in combination with LV.NAGLU, to understand the importance of inflammation on behaviour. NAGLU enzyme was substantially increased in the brain of LV.NAGLU and LV.NAGLU-IGFII-treated mice, with little expression in wild-type bone marrow transplanted mice. LV.NAGLU treatment led to behavioural correction, normalisation of heparan sulphate and sulphation patterning, reduced inflammatory cytokine expression and correction of astrocytosis, microgliosis and lysosomal compartment size throughout the brain. The addition of prednisolone improved inflammatory aspects further. Substantial correction of lysosomal storage in neurons and astrocytes was also achieved in LV.NAGLU-IGFII-treated mice, despite limited enzyme secretion from engrafted macrophages in the brain. Interestingly both wild-type bone marrow transplant and prednisolone treatment alone corrected behaviour, despite having little effect on brain neuropathology. This was attributed to a decrease in peripheral inflammatory cytokines. Here we show significant neurological disease correction is achieved using haematopoietic stem cell gene therapy, suggesting this therapy alone or in combination with anti-inflammatories may improve neurological function in patients.

Keywords

Gliosis

Lysosomal storage disease

Microglia

Mucopolysaccharidosis

Neurodegeneration

Abbreviations

AAV	Adeno-associated virus
β-Hex	β-*N*-acetyl hexosaminidase
BM	Bone marrow
CFU	Colony forming unit
CNS	Central nervous system
CS	Chondroitin sulphate
DS	Dermatan sulphate
GalNAc	*N*-acetyl-galactosamine
GlcNAc	*N*-acetyl-glucosamine
GlcNS	*N*-sulpho-glucosamine
HS	Heparan sulphate
HSC	Haematopoietic stem cell
HSCGT	Haematopoietic stem cell gene therapy
HSCT	Haematopoietic stem cell transplant
IB4	Isolectin B4
IGFII	Insulin-like growth factor 2
LV	Lentiviral vector
MPS	Mucopolysaccharidosis
NAGLU	α-*N*-acetylglucosaminidase
PRED	Prednisolone
SGSH	*N*-sulfoglucosamine sulfohydrolase
VCN	Vector copy number

WBC	White blood cell
WT	Wild-type
ΔUA	Uronic acid

Introduction

Mucopolysaccharidosis IIIB (MPSIIIB or Sanfilippo B syndrome) is a neurodegenerative lysosomal storage disease caused by a deficiency in the glycosaminoglycan degrading enzyme, α-*N*-acetylglucosaminidase (NAGLU). NAGLU deficiency results in the global accumulation of partially degraded heparan sulphate (HS) in cells, leading to cellular dysfunction which is particularly apparent in the brain. Symptom onset begins within the first two to four years of life, characterised by a plateau in development, speech delay, and worsening behavioural problems, together with minor somatic indicators such as organomegaly and facial dysmorphia. Progressive motor impairment follows leading to greatly shortened life expectancy. There are currently no effective treatments.

Enzyme replacement therapy has successfully treated somatic disease in other MPS disorders. Cross-correction occurs via mannose-6-phosphate mediated enzyme uptake by deficient cells. However the inability of delivered enzyme cannot to cross the blood brain barrier limits its worth in MPSIIIB, where the main pathology is neurological. Approaches to deliver enzyme via an intracerebroventricular route are in progress, but these methods are invasive. A C-terminal fusion of NAGLU to insulin-like growth factor 2 (rhNAGLU-IGFII), which also binds the mannose-6-phosphate-receptor leads to more efficient uptake, lysosomal targeting and activity following intracerebroventricular injection in MPSIIIB mice (Kan *et al.*, 2014a; Kan *et al.*, 2014b).

Another option for MPSIIIB patients is delivery of adeno-associated virus (AAV) based gene therapy vectors via a variety of routes to treat the brain (Fu *et al.*, 2002; Cressant *et al.*, 2004; Fu *et al.*, 2007; Fu *et al.*, 2010). One hurdle in developing these therapies is achieving effective vector distribution from the sites of injection, something that can be effectively achieved in rodents but not in patients to date (Tardieu *et al.*, 2014; Tardieu *et al.*, 2017).

Haematopoietic stem cell transplant (HSCT), enables donor HSCs to repopulate bone marrow (BM) of myeloablated recipients, with donor-engrafted leukocytes secreting enzyme to cross-correct somatic cells. BM-derived monocytes are also able to cross the blood-brain barrier and

engraft within the brain, enabling cross-correction within the central nervous system (CNS). Although effective in MPSI patients, several studies have shown poor neurological outcomes following HSCT in MPSIIIB patients (Vellodi *et al.*, 1992; Shapiro *et al.*, 1995), despite successful clearance of HS in somatic organs. This failure is thought to be due to poor endogenous secretion of NAGLU from engrafted donor macrophages in the brain. Cord blood transplantation has had greater success in MPSIIIB patients (Prasad *et al.*, 2008), but behaviour is not corrected, despite improved survival. A retroviral mediated HSC gene therapy (HSCGT) approach in MPSIIIB mice, designed to overcome this failing was found to have disappointing efficacy and the effect reduced with time (Zheng *et al.*, 2004).

We have previously demonstrated in the clinically similar disease MPSIIIA, that *ex vivo* gene delivery of *N*-sulphoglucosamine sulphohydrolase (SGSH) to HSCs using a clinically approved lentiviral vector (LV), driven by the myeloid specific CD11b promoter, led to restoration of 11% wild-type (WT) activity of SGSH in the brains of MPSIIIA mice, normalised HS storage and CNS pathology and corrected behaviour (Sergijenko *et al.*, 2013), whereas WT transplantation was unsuccessful (Langford-Smith *et al.*, 2012). CD11b is highly expressed by monocyte/macrophage/microglial cells, leading to enhanced transgene expression in the brain compared to the ubiquitous phosphoglycerate kinase promoter. This approach is now under development for clinical trial (Bigger and Wynn, 2014).

We applied this HSCGT methodology in the MPSIIIB mouse model, comparing MPSIIIB mice receiving WT HSCs versus MPSIIIB HSCs transduced with a vector expressing either NAGLU (LV.NAGLU) or a poorly secreted version of NAGLU fused to IGFII (LV. NAGLU-IGFII) (Kan *et al.*, 2014b). This allowed us to study the role of NAGLU expressing donor macrophages in the brain, including the inflammatory cytokine/chemokine effects that they mediate, in the context of limited NAGLU secretion.

There are several anti-inflammatories now used clinically to manage abnormal behaviour (Reale *et al.*, 2012; Felger and Lotrich, 2013). Given that peripheral cytokines impact directly on brain pathology, prednisolone (PRED), a corticosteroid that has limited ability to cross the blood-brain barrier, was used to treat MPSIIIB mice to test the effect of somatic correction of inflammation on brain disease. Notably however, prednisolone is not recommended in patients due to significant side effects, not seen in rodents. A combined PRED and LV.NAGLU HSCGT group was also included. We demonstrate significantly increased brain NAGLU activity, normalised HS brain storage, reduced neuroinflammation and secondary storage and behavioural correction with LV-mediated HSCGT using both vectors, highlighting the

effectiveness of our LV.NAGLU vector approach for correction of brain disease in MPSIIIB. No brain correction was seen following WT HSCT. PRED treatment additionally reduced somatic tissue inflammation, providing enhanced patient benefit when used in combination with LV.NAGLU HSCGT, but all treatments improved hyperactive behaviour.

Materials and Methods

Generation and *in vitro* testing of LV.NAGLU and LV.NAGLU-IGFII

Codon optimised human NAGLU (GenBank® accession number NM_000263.3) flanked with attB1 and attB2 sites (manufactured by GeneArt) was cloned using the gateway system (Life Technologies) into the pCCL LV backbone downstream of the CD11b promoter (Sergijenko *et al.*, 2013), to generate pCCLsin.cPPT.hCD11b.NAGLU.WPRE (LV.NAGLU). NAGLU-IGFII fusion plasmid comprising full length NAGLU, a short unstructured linker, the c-Myc epitope EQKLISEED and amino acids 32-91 of IGFII (GenBank® accession number NM_001007139.4) was kindly donated by Patricia Dickson (Kan *et al.*, 2014b). PCR, using extended primers designed to incorporate AttB1 and AttB2 sites either side of NAGLU-IGFII, was used to amplify the NAGLU-IGFII segment, which was then agarose gel purified and cloned using the gateway system into the LV genome plasmid described above to generate pCCLsin.cPPT.hCD11b.NAGLU-IGFII.WPRE (LV.NAGLU-IGFII). A GFP LV in the same vector backbone (pCCLsin.cPPT.hCD11b.eGFP) was used as a control (Langford-Smith *et al.*, 2012). LV was produced and titred as described previously (Langford-Smith *et al.*, 2012; Sergijenko *et al.*, 2013). CHME3 cells were transduced at a multiplicity of infection of 10, collecting media and cells after 48 hours.

Mice, HSC isolation, transduction and transplantation

All *in vivo* procedures were ethically approved in accordance with Home Office regulations. Mice were housed in a 12/12-hour light/dark cycle with food and water provided *ad libitum*. MPSIIIB (B6.129S6-*Naglu*^{tm1Efn}/J, strain 003827, Jackson Laboratory) mice were backcrossed with C57BL/6J mice (CD45.2) or B6.SJL-*Ptprc*^{a} *Pepc*^{b}/BoyJ (strain 002014, Jackson Laboratory, CD45.1) mice to distinguish between donor and recipient haematopoietic cells. BM was isolated from donor CD45.1-MPSIIIB mice, lineage depleted and HSCs transduced with a multiplicity of infection of 60 as described previously (Langford-Smith *et al.*, 2012). Recipient mice at 2 months of age were treated with intraperitoneal 125mg/kg busulfan

(Busilvex; Pierre Fabre, Boulogne, France) over 5 days prior to tail vein injection of $3x10^5$ LV-transduced HSCs. Whole BM from CD45.1-WT mice ($1x10^7$) was injected into busulfan-conditioned MPSIIIB mice for WT HSCT treated mice. PRED was added at 6mg/L (~1mg/kg per day) in drinking water from 6 weeks in control mice or 14 weeks following LV-mediated HSCGT. The survival curve was limited by home office licence regulations, meaning that mice had to be culled when they showed significant signs of disease; typically urine retention and loss of body condition. A cohort of untreated WT littermates suffered from alopecia (without other signs of distress) from 13 months, requiring sacrifice.

Donor chimerism

HSC engraftment was assessed in peripheral blood following staining with anti-mouse CD45.1-PE (donor) and CD45.2-FITC (recipient) (both BD Pharmingen) antibodies and analysed on a BD FACS Canto II flow cytometer. Animals where chimerism was below 60% were excluded.

Tissue harvesting

At 8-months of age, mice were anaesthetized, the right atrium cut to allow blood collection into citrate buffer for plasma and white blood cells (WBCs) and transcardially perfused with warmed PBS to remove blood, as described previously (Langford-Smith *et al.*, 2012). One brain hemisphere and liver pieces were fixed in 4% paraformaldehyde for 24 hours, before washing with PBS. Brain hemispheres were placed into 30% sucrose 2mM $MgCl_2$ for 24 hours before freezing at -80ºC for 30µm coronal microtomy. Liver was transferred into 70% ethanol for paraffin mounting and slicing. The second brain hemisphere and remaining organs were frozen at -80ºC. BM was isolated from the hind legs of mice and set up in MethoCult culture (Stem Cell Technologies) as previously described (Langford-Smith *et al.*, 2012) to assess CFU lineage development.

Vector copy number determination

Vector copy number (VCN) was determined from harvested tissue using quantitative PCR as described (Langford-Smith *et al.*, 2012).

Enzyme assays

Tissue was homogenised in 0.5M NaCl/0.02M Tris, 0.1% v/v Triton X-100, pH7-7.5, then centrifuged at 2200g, storing the supernatant. Protein concentration was determined using Pierce BCA assay kit (Fisher Scientific, Loughborough, UK). For NAGLU enzymatic assay, 10-60μg of total protein was incubated with NAGLU substrate (4-methylumbelliferyl-*N*-acetyl-α-D-glucosaminide, Sigma) for 4 hours at 37°C, resulting in release of fluorescent 4-methylumbelliferone. Stop buffer (0.2M carbonate buffer, pH 9.5) was then added and the fluorescence measured immediately at excitation 360 nm and emission 460 nm using a Synergy HT Microplate reader (BioTec, Potton, UK) against known 4-methylumbelliferone standards. For assessment of β-Hex activity 1-2μg total protein was incubated with 4-Methylumbelliferyl-*N*-acetyl-β-D-glucosaminide for 40 minutes at 37°C. Stop buffer was then added and the fluorescence measured.

Glycosaminoglycan analysis

Brain and liver samples were homogenised in PBS/1% Triton X-100 and a small sample taken for protein quantification. Tissues were digested with pronase (Roche) and glycosaminoglycans purified as described previously (Holley *et al.*, 2011). Glycosaminoglycan samples were then divided into two; one aliquot was digested with heparinase I/II/III and labelled with 2-aminoacridone as described previously (Holley *et al.*, 2011), the second was digested with 2mIU chondroitinase ABC (Sigma) and 2-aminoacridone labelled. Both HS and chondroitin sulphate/dermatan sulphate (CS/DS) disaccharides were subject to RP-HPLC using a Zorbax Eclipse XBD-C18 column (Agilent) equilibrated in 95% 0.1M ammonium acetate/5% acetonitrile, running on an Agilent 1200 Series HPLC system. Disaccharides were eluted over a 5-20% gradient of acetonitrile at 0.2 mL/min, detecting in-line fluorescence at excitation 425nm and emission 520nm. 2-aminoacridone-labelled CS/DS or HS disaccharide standards (Iduron) were used for peak identification. For calculation of μg HS or CS/DS, total fluorescence was compared with the fluorescence from known quantities of HS or DS. Correction factors were calculated (Supplementary Table 1) as described (Deakin and Lyon, 2008).

Measurement of cytokine/chemokine level

MIP-1α (CCL3), IL-1α, MCP-1 (CCL2), KC (CXCL1) and RANTES (CCL5) were measured in brain, liver and plasma using Cytomeric Bead Array flex sets (BD Biosciences) according to manufacturer's instructions.

Open field behaviour

Open field behaviour was performed as previously described (Langford-Smith *et al.*, 2011a; Langford-Smith *et al.*, 2011b). The data were analysed using Ethovision XT11.5 software (Noldus).

Immunohistochemistry

Free-floating immunohistochemistry was performed on seven coronal brain sections (30μm) from matched areas of Bregma (0.98, 0.14, −0.46, −1.06, −1.70, -2.40 and −3.28mm) as described previously (Malinowska *et al.*, 2010; Sergijenko *et al.*, 2013). Paraffin embedded liver sections (5μM) were dewaxed and rehydrated prior to staining, processing as above. Primary antibodies included rat anti-LAMP2 (Abcam), rabbit anti-NeuN (Abcam), peroxidase-conjugated BSI-B4 (Sigma), rabbit anti-GFAP (DakoCytomation), and mouse anti-GM2 (a gift from Dr Konstantin Dobrenis); secondary antibodies included goat anti-rabbit Alexa Fluor® 594, goat anti-rat Alexa Fluor® 488 (Life Technologies) and Biotinylated-goat anti-mouse IgM (Vector laboratories). DAPI was used to highlight nuclei. IB4 stained slides were counterstained with Mayer's haemotoxylin. Images were acquired on a 3D-Histech Pannoramic-250 microscope slide-scanner using a 20x/0.30 Plan Achromat objective (Zeiss) and the DAPI, FITC and TRITC filter sets and processed using Case Viewer software (3D-Histech).

Experimental design

Four experimental groups were compared against WT or MPSIIIB control mice. 14-22 mice were analysed for behaviour and 6-10 for biochemistry and histology. N numbers were based on previous power calculations as seen in the MPSIIIA mouse model (Sergijenko 2013) and behavioural changes in the MPSIIIB mouse model (Langford-Smith 2011). It was impossible to blind *in vivo* treatment groups, due to the nature of the mouse model, treatments given and experiment size, with transplants staggered over several months, yet treatment groups were filled equally to avoid bias. Analysis was carried out in a blinded fashion.

Statistical analysis

GraphPad Prism was used for one-way or two-way analysis of variance (ANOVA) and Tukey *post hoc* test for analysis. Significance was $P<0.05\%$.

Results

Efficient expression of NAGLU from lentiviral vectors

We constructed a lentiviral vector expressing either human NAGLU or human NAGLU fused to amino acids 32–91 of IGFII (Kan *et al.*, 2014b), both under the control of the myeloid specific CD11b promoter (Fig. 1A). Over-expression of active NAGLU enzyme was confirmed in the human microglial cell line CHME3, using LV.eGFP as a control. Significant increases of 5.5-fold and 6.2-fold in intracellular NAGLU activity was seen with LV.NAGLU and LV.NAGLU-IGFII respectively (Fig. 1B), without noticeable toxicity. Secreted activity was increased 9.9-fold with LV.NAGLU but minimal secretion was observed with LV.NAGLU-IGFII (Fig. 1C), providing us with a tool to study the effect of restricting NAGLU expression to engrafted cells, with little cross-correction of neighbouring cells.

In order to determine whether *ex vivo* transduction of MPSIIIB HSCs can effectively treat the mouse model of MPSIIIB following transplant, we set up seven treatment groups *in vivo* (Fig. 1D): 1) WT control, 2) MPSIIIB control, 3) WT HSCT in MPSIIIB mice, 4) LV.NAGLU-transduced MPSIIIB HSCs in MPSIIIB, 5) LV.NAGLU-IGFII-transduced MPSIIIB HSCs in MPSIIIB, 6) PRED in MPSIIIB, and 7) LV.NAGLU-transduced MPSIIIB HSCs combined with PRED in MPSIIIB (PRED+LV.NAGLU). Thus groups 4, 5 and 7 (LV.NAGLU, LV.NAGLU-IGFII and PRED+LV.NAGLU) all received LV-mediated HSCGT. Although prednisolone has some deleterious effects in children, it was chosen over other anti-inflammatories due to its ease of long-term administration in drinking water compared to the need for daily injections, and its previous efficacy in MPSIIIB animals (DiRosario *et al.*, 2009). Average VCN measured in HSC-enriched BM at transplant was similar at 7.4-10.8 VCNs per cell (Fig. 1E). Consequently, NAGLU activity in HSC-enriched BM was substantially increased above WT levels in all LV-mediated HSCGT groups (8.4-fold over WT in LV.NAGLU, 8.9-fold in LV.NAGLU-IGFII, and 7.6-fold in PRED+LV.NAGLU) with no significant differences between groups (Fig. 1F). Equally there were no significant differences in the total number of CFUs or the proportion of each colony type obtained from WT, MPSIIIB or MPSIIIB HSCs transduced with either LV vector (Fig. 1G/H), suggesting no NAGLU or LV toxicity in HSCs. Over 82% donor peripheral blood chimerism was achieved in all transplant groups at 6 months of age, with no significant difference between groups (Fig. 1I).

A proportion of mice in each group were culled at 8 months of age to assess efficiency of therapy. Remaining mice were kept for long-term analysis, sacrificing at their humane

endpoint. Mean survival was 9.4 months in untreated MPSIIIB mice and PRED treated mice (Fig. 1J/K), typically due to urine retention as seen previously (Gografe *et al.*, 2009). Survival was significantly increased in WT HSCT and LV-mediated HSCGT groups, with reduced incidence of urine retention.

LV-mediated HSCGT results in significantly increased NAGLU activity compared to WT HSCT

Mice sacrificed at 8 months of age were used for biochemical and immunohistological analysis. There was no significant difference in the total number of BM-derived CFUs (Supplementary Fig. 1A) or in the percentage of CFUs of different lineage types (Supplementary Fig. 1B) suggesting no toxicity of transgene or vector.

VCN and NAGLU activity were measured in WBCs, plasma, BM, brain, spleen and liver (Fig. 2). No significant differences in VCN were seen between LV-mediated HSCGT treatment groups in WBCs, BM, brain or liver, however in all organs tested there was a trend towards higher VCNs in the LV.NAGLU group versus PRED+LV.NAGLU (Fig. 2/Supplementary Fig. 2). A significant difference between groups was seen in spleen, with 10 VCNs in the LV.NAGLU group compared to 4.3 in PRED+LV.NAGLU. This is likely due to the reduced VCN in transplanted HSCs between these groups (Fig. 1E).

No detectable NAGLU enzyme activity was found in MPSIIIB tissues. All treatments except PRED increased NAGLU activity compared to untreated MPSIIIB. NAGLU activity was increased in WBCs to 221% of WT in WT HSCT animals, compared to 3741%, 1853% and 1905% in LV.NAGLU, LV.NAGLU-IGFII and PRED+LV.NAGLU groups respectively (Fig. 2B). Plasma NAGLU levels were 287% of WT with LV.NAGLU, but only 14% of WT was seen in LV.NAGLU-IGFII animals, suggesting little secretion of NAGLU-IGFII occurs *in vivo* (Fig. 2D), mirroring results *in vitro* (Fig. 1C). Little plasma NAGLU was apparent in WT HSCT animals, suggesting that native NAGLU secretion is low from haematopoietic cells. BM NAGLU activity was increased to 89% of WT with WT HSCT and 175% of WT in LV.NAGLU-IGFII (Fig. 2G). Substantially increased BM NAGLU levels were seen in LV.NAGLU and LV.NAGLU+PRED groups (1240% and 780% respectively). Positive correlations were seen between VCN and enzyme overexpression (Supplementary Fig. 2).

Brain NAGLU activity was only increased significantly compared to MPSIIIB in LV-mediated HSCGT groups (Fig. 2J). 1.3% of WT NAGLU levels were seen with WT HSCT, compared

to 13% with LV.NAGLU and 8.6% with LV.NAGLU-IGFII. 6.0% enzyme activity was achieved in PRED+LV.NAGLU groups, probably reflecting the respective VCN in transplanted HSCs (Fig. 2I, 1E). In spleen and liver, all treatments increased NAGLU enzyme levels, with the greatest correction achieved with HSCGT (Fig. 2M/P).

Lysosomal function is important to maintain cellular homeostasis, with increased lysosomal size often leading to dysregulated expression of other lysosomal enzymes (Sardiello *et al.*, 2009). MPSIIIB mice exhibited increased β-Hex activity over WT in all tissues examined (Fig. 2C/E/H/K/N/Q). Both WT HSCT and LV-mediated HSCGT transplant groups exhibited a reduction in β-Hex in somatic tissues. However, significant reductions in β-Hex in the brain were only seen in LV-mediated HSCGT groups (Fig. 2K), paralleling the upregulation of NAGLU seen in the brain of these animals.

Normalisation of glycosaminoglycan storage in the brains of LV-mediated HSCGT treated mice

Loss of NAGLU results in the accumulation of partially degraded HS, therefore primary HS storage was measured in the liver and brain of control and treated mice to determine the effectiveness of therapy (Fig. 3/Supplementary Fig. 3). In the liver a 21-fold increase in HS was seen in MPSIIIB mice, which was normalised to near WT levels in both WT HSCT and all HSCGT treatment groups (Fig. 3A). However, in the brain, only LV-mediated HSCGT groups showed normalised HS storage, with only a marginal non-significant decrease in WT HSCT mice (Fig. 3C). A slight decrease in accumulated HS in liver and brain was also seen with PRED treatment, but this was non-significant (Fig. 3A).

Analysis of the HS disaccharide composition revealed abnormalities in several sulphated disaccharide units in MPSIIIB mice in both liver (Fig 3B) and brain (Fig 3D). In the brain 76% of all disaccharides were *N*-sulphated (Supplementary Fig. 3B), coupled with 2.7-fold and 2.0-fold increases in 2-*O*-sulphation and 6-*O*-sulphation respectively. Consistent with reductions in HS levels, brain HS patterning was only corrected with LV-mediated HSCGT, whereas liver HS patterning and sulphation was normalised in all HSCGT and WT HSCT groups (Fig. 3/Supplementary Fig. 3). These dramatic increases in total HS and in HS sulphation in MPSIIIB are likely to present both a physical and functional barrier to normal cellular function. Thus normalisation of brain HS storage and patterning following HSCGT should restore HS-protein binding homeostasis.

NAGLU enzyme is not directly involved in CS/DS degradation, however secondary storage of other lysosomal substrates might be expected, therefore we measured CS/DS in the liver and brain of control and treated animals. The main disaccharide CS/DS units found in the liver were ΔUA-GalNAc(4S,6S) and ΔUA-GalNAc(4S), with few 2-*O*-sulphate-containing residues (Fig. 3/Supplementary Fig. 3). 6-*O*-sulphation was significantly increased in MPSIIIB animals together with a 4.1-fold increase over WT in total CS/DS. Total CS/DS was significantly decreased in the liver of both WT-HSCT and all HSCGT groups and interestingly, also those treated with PRED alone (Fig. 3E). Normalisation of 6-*O*-sulphation levels was also apparent in all transplant groups, however CS/DS patterning was not corrected in PRED mice (Fig. 3F), despite the decrease in CS/DS burden.

In the brain, the major CS/DS component is ΔUA-GalNAc(4S) with no detectable 2-*O*-sulphation and few 6-*O*-sulphate containing disaccharides. No secondary storage of CS/DS or alterations in CS/DS sulphation were apparent between WT and MPSIIIB animals (Fig. 3H/Supplementary Fig. 3D).

Inflammatory cytokines are only reduced in the brain of LV-mediated HSCGT-treated mice

Lysosomal accumulation of HS and secondary storage products lead to inflammation, with many chemokines/cytokines binding directly to HS, leading to their capture at the cell surface. Significant upregulation of MIP-1α, IL-1α, MCP-1 and KC protein was noted in the brain of MPSIIIB mice at 8-months of age (Fig. 4A-D). WT HSCT resulted in little or no effect on these levels. Prednisolone treatment alone had no effect on these cytokines in the brain. LV-mediated NAGLU overexpression using either LV-vector in all HSCGT groups resulted in complete normalisation of MIP-1α, IL-1α and MCP-1 in the brain (Fig. 4A-C), with expression reduced to WT levels.

A reduction in inflammatory chemokines was also seen in the periphery; liver MIP-1α, IL-1α, MCP-1, KC and RANTES and circulating plasma IL-1α, MCP-1 and KC were reduced in all LV-mediated HSCGT groups, as well as in WT HSCT mice, probably due to the normalisation of HS levels in the periphery. Mice that received the anti-inflammatory prednisolone also exhibited significantly suppressed levels of these inflammatory cytokines in the liver and plasma, indeed dropping below WT. Additional reductions in cytokine levels were seen with PRED+LV.NAGLU in the periphery, suggesting synergistic effects of combined treatments.

This highlights that although PRED does not appear to directly affect brain inflammation, it acts to significantly reduce inflammation in the periphery.

LV-mediated HSCGT, HSCT and PRED each significantly improve behaviour

MPSIIIB patients exhibit increasingly severe behavioural problems as a result of accumulating neurological damage. To determine whether LV-mediated HSCGT treatment was able to ameliorate the behavioural phenotype seen in MPSIIIB mice, the open field test was conducted at 6 months of age (4 months post-transplant). Consistent with previous findings, MPSIIIB mice display a hyperactive phenotype (Langford-Smith *et al.*, 2011b), behaving significantly different from WT in the four parameters tested: total distance moved, frequency of centre entries, frequency immobile and average speed (Fig. 4M-P). Interestingly, all treatments, including WT HSCT and PRED, where brain inflammation remains high, resulted in full correction of these behavioural phenotypes, with animals appearing indistinguishable from WT (Fig. 4M-P). Additionally improvement in these behaviours observed in PRED-treated mice, was further ameliorated with the addition of LV.NAGLU (Fig. 4M-O), suggesting additional benefit with combined treatments.

Only LV-mediated HSCGT is sufficient to correct astrogliosis and microgliosis in the brain

Maintenance of the neuron-microglia-astrocyte "triad" is critical for normal brain function (Cerbai *et al.*, 2012), yet enlarged lysosomes and chronic neuroinflammation with extensive microgliosis and astrocytosis is characteristic of MPSIIIB disease (Wilkinson *et al.*, 2012). Coronal brain sections were stained with lysosomal associated membrane protein 2 (LAMP2) to highlight lysosomal swelling, together with either activated astrocyte marker GFAP (Fig. 5/Supplementary Fig. 4) or neuronal marker NeuN (Fig. 6). In WT, astrocytic GFAP+ cells were largely absent from the cortex, striatum and thalamic regions, although staining was clearly visible in the stratum layers of the hippocampus and amygdala (Fig. 5/Supplementary Fig. 4). In contrast, significant astrocytosis was apparent throughout the MPSIIIB brain, with large numbers of activated astrocytes present in the cortex, striatum and substantia nigra. No obvious changes in neuronal cell number were noted between WT and MPSIIIB following staining for NeuN, indicating there is little neuronal cell loss in MPSIIIB (Fig. 6).

In WT brains LAMP2, staining was punctate and more peripheral within neurons, with negligible astrocytic expression. MPSIIIB mice however exhibit significantly increased LAMP2 staining compared to WT, with intense large vesicular LAMP2+ lysosomes present throughout GFAP+ astrocytes and in distinct locations around the nucleus of NeuN+ neurons within the cortex, pyramidal regions of the hippocampus and throughout the amygdala (Fig. 5/6). In the striatum and substantia nigra intense LAMP2 staining appeared restricted to GFAP+ astrocytes (Fig. 5). Thus although there is no change in neuronal cell number the significant lysosome burden in these cells is likely to dramatically alters cellular function, leading to the neurological outcomes noted in these mice.

PRED treatment resulted in minimal changes in LAMP2 staining or astrocytosis (Fig. 5). A small reduction in the intensity of LAMP2 was present in the cortex of WT HSCT mice (Fig. 5A/C), although no significant decreases in other regions of the brain compared to untreated MPSIIIB were apparent. In HSCGT mice treated with LV.NAGLU with or without PRED treatment or following treatment with LV.NAGLU-IGFII, significant reductions in LAMP2 staining were apparent, with little astrocytosis (GFAP+ cells) noted throughout the cortex, striatum and all other regions of the brain studied (Fig. 5/Supplementary Fig. 4). LV.NAGLU consistently gave greater reductions in lysosomal swelling compared to LV.NAGLU.IGFII but both treatments mediated reductions in lysosomal swelling in neurons and astrocytes indicating cross-correction.

Severe neuroinflammation and microgliosis in MPSIIIB is highlighted by a 47-fold increase in isolectin B4 (IB4)-positive microglia in the cortex and extensive staining throughout the MPSIIIB brain (Fig. 7A-C/Supplementary Fig. 5). WT HSCT resulted in a small, yet significant decrease in IB4 staining however levels were still 33-fold over WT. Little effect on brain microgliosis was seen with PRED treatment. MPSIIIB mice treated with LV.NAGLU with or without PRED resulted in complete reversal of neuroinflammation, with few IB4+ cells remaining in the cortex, striatum or hippocampal brain regions (Fig. 7). IB4+ cells did however remain in the amygdala, thalamic and substantia nigra regions of the brain in these mice (Supplementary Fig. 5), although levels were substantially reduced compared to untreated animals. The amygdala is important in memory processing and emotional responses, thus reductions in IB4+ cells might be key for amelioration of behavioural issues. The level of correction achieved with LV.NAGLU-IGFII was not as pronounced as with LV.NAGLU, whereby IB4+ cell numbers remained elevated compared to WT. However, microgliosis in

LV.NAGLU-IGFII animals was significantly improved compared to untreated and WT HSCT (Fig. 7A-C).

MPS disease is also characterised by secondary storage of other compounds including GM2 gangliosides in the brain, which may itself propagate CNS inflammatory responses observed in GM2 mice (Jeyakumar *et al.*, 2003). WT animals exhibit little GM2 storage in the brain (Fig. 7D-F/Supplementary Fig. 5). However MPSIIIB animals have distinct punctate storage within layers V/VI of the cortex, throughout amygdala and hippocampal regions and in the zona incerta. GM2 staining was absent or low in all LV-mediated HSCGT treated mice, appearing indistinguishable from WT controls, however only marginal reductions in staining was seen in WT HSCT mice. No apparent changes in GM2 staining were seen with PRED treatment alone. Therefore staining of the brain for neuroinflammatory markers suggests LV-mediated HSCGT can abrogate the disease phenotype in MPSIIIB animals.

PRED treatment reduces inflammation in the liver

Although no reduction in inflammation was seen in the brain of PRED treated mice, consistent with prednisolone being unable to cross the blood-brain barrier, cytokine analysis suggested widespread reductions in inflammatory cytokine expression in the periphery. Therefore liver from control and treated mice was stained with IB4 (Fig. 8). Intense IB4 staining was visible throughout the liver of untreated MPSIIIB mice compared to WT. PRED treatment resulted in significant decreases in IB4-reactivity throughout the liver, with levels similar to WT. WT HSCT and HSCGT-treated groups also exhibited significantly reduced IB4+ staining, however combined PRED+LV.NAGLU treatment resulted in synergistic results, with levels dropping below WT (Fig. 8). This suggests prednisolone may aid reduction in disease pathology in somatic organs.

Discussion

Here we demonstrate a LV-mediated HSCGT approach to treat neuropathology in Sanfilippo disease, providing a promising treatment option for these patients. WT HSCT, although providing benefit to somatic organs and increasing life span, provided insufficient NAGLU levels in the brain to improve neuropathology, as seen previously (Zheng *et al.*, 2004; Heldermon *et al.*, 2010). This is similar to outcomes in Sanfilippo patients, who typically have improved lifespan without neurological correction (Vellodi *et al.*, 1992; Prasad *et al.*, 2008).

In contrast HSCGT with LV.NAGLU-transduced autologous HSCs improved all pathogenic markers, resulting in normalisation of primary HS storage, abolition of secondary substrate storage materials and significant reductions in inflammatory cytokine expression, lysosomal swelling, microgliosis and astrogliosis in the brain. Enzyme levels achieved in somatic organs were also far superior to WT HSCT. In this study mice were treated at approximately 2 months of age, at which stage considerable disease burden exists (Wilkinson *et al.*, 2012; Ribera *et al.*, 2015). Thus our LV-mediated HSCGT approach is able to successfully correct disease pathology, even when significant neuropathology already exists. Significantly in HSCGT-treated animals, restoration of brain NAGLU enzyme above ~5% appeared sufficient for complete reversal of the MPSIIIB neuropathology at 6 months post-treatment. This is in contrast to a retroviral HSCGT approach previously tested in MPSIIIB (Zheng *et al.*, 2004), where brain correction was sporadic, with ~25% WT brain enzyme in the highest group, but with considerable variability, with brain expression in most animals remaining low. Probable gene silencing from the LTR promoter was noted, reflecting the early generation vector design and transduction methodology employed.

C-terminal fusion of IGFII to NAGLU resulted in minimal NAGLU secretion into the culture medium of CHME3 microglial cells *in vitro* or into blood plasma *in vivo*. This is in contrast to previous results in Chinese hamster ovary cells (Kan *et al.*, 2014b), yet considering the identical linker was used, this most likely reflects the differences in cell types used. Regardless, it is typically assumed that cross-correction is the major mechanism for disease correction and is essential for treatment efficacy. However, restricting expression of NAGLU to the engrafted donor macrophages in the brain and thus limiting cross-correction with LV.NAGLU-IGFII, surprisingly resulted in significant reductions in neuropathology, with near identical outcomes to using the unmodified LV.NAGLU vector. Although we cannot exclude that some cross-correction remains, and that the IGFII linker may enhance uptake (Kan *et al.*, 2014b), despite reduced secretion, as observed by reductions in neuronal and astrocytic LAMP2, these data nevertheless suggest that correction of donor macrophages may prove as important for efficient brain correction as widespread dissemination of NAGLU to all cell types in the brain.

We were surprised that WT HSCT and PRED were able to improve hyperactivity, correcting behavioural phenotypes seen in MPSIIIB mice. However this is consistent with previous findings in which treatment of MPSIIIB mice where prednisolone improved performance in the Morris Water Maze, significantly reduced spleen size and decreased T-cell activation (DiRosario *et al.*, 2009). Whereas WT HSCT effectively delivers NAGLU enzyme to somatic

organs, abolishing accumulated HS and thereby restoring lysosomal function, the corticosteroid prednisolone acts as an anti-inflammatory. Common to both treatments is significantly reduced inflammation in the periphery, but without central brain effects. Several other studies have indicated that correction of somatic inflammation has the potential to treat disorders of neurodevelopmental origin. For example in the lysosomal storage disease infantile neuronal ceroid lipofuscinosis, intraperitoneal injections of MW151, a small-molecule anti-neuroinflammatory, was able to reduce the incidence of seizures, despite having little effect on brain pathology (Macauley *et al.*, 2014). Prednisolone itself is not recommended as a long-term treatment for patients due to deleterious side effects. However, our data linking a decrease in circulating inflammatory cytokines with improved behaviour indicates that treatments with a similar action to prednisolone may provide relief from at least some of the behavioural aspects of MPSIIIB disease, and has the potential to be an adjunct therapy. Although LV-mediated HSCGT alone appears sufficient to correct the CNS pathology, the benefits of prednisolone to somatic disease indicates that specifically targeted anti-inflammatories could be incorporated into therapeutic approaches for MPSIIIB.

Several other strategies to treat MPSIIIB patients are being trialled. Intracerebroventricular injection of NAGLU enzyme has proven effective in mouse models of MPSIIIB (Kan *et al.*, 2014a) but clinical application of this approach in MPS II has been fraught with device failure issues (Muenzer *et al.*, 2016), with half of the enrolled patients required surgical intervention due to delivery device failure. A similar trial for MPSIIIA was unsuccessful (Jones *et al.*, 2016). A systemic gene therapy approach using intravenous injection of AAV9 in mice at 1 month of age was reported to achieve greater than 2-fold over WT brain enzyme delivery, together with somatic NAGLU expression, glycosaminoglycan reduction and behavioural correction (Fu *et al.*, 2011; Fu *et al.*, 2017). This approach has now been approved for a phase 1/2 clinical trial in MPSIIIB patients (IND 16671). Nonetheless scalability remains a major challenge, requiring a significant change in manufacturing infrastructure to enable the synthesis of sufficient virus at the magnitude required to treat patients.

Targeted injection of AAV-NAGLU vectors directly into the brain of MPSIIIB mice has also been tested, leading to long-term NAGLU expression, reduced glycosaminoglycan levels and some behavioural improvements (Fu *et al.*, 2002; Cressant *et al.*, 2004; Fu *et al.*, 2007; Fu *et al.*, 2010; Heldermon *et al.*, 2010; Heldermon *et al.*, 2013). However cellular transduction was often restricted to those cells surrounding the injection site and systemic organs remain uncorrected, something that is overcome by our HSCGT approach, as donor macrophages

distribute and engraft throughout the brain and somatic organs (Wilkinson *et al.*, 2013). Interestingly in some studies survival was increased to 19-20 months for some animals, above what we achieve here with HSCGT. The significance of survival is however not clear in MPSIIIB, where the main disease pathology is in the brain. In the absence of significant neuronal cell death in the mouse model, the endpoint is typically urine retention (Gografe *et al.*, 2009). Scalability with the AAV approach does seem to be problematic, with substantial increases in vector distribution and injection sites required for significant success in patients (Tardieu *et al.*, 2017). An alternative is direct injection of AAV9-NAGLU into cerebrospinal fluid, reported to result in widespread CNS-targeting and some somatic correction via vector passage into circulation (Ribera *et al.*, 2015). The high rate of pre-existing immunity to AAV vectors in the human population however provides a significant obstacle for therapy, with patients often positive for neutralising-antibodies against multiple serotypes (Hareendran *et al.*, 2013). Generation of novel AAV-serotypes is therefore essential.

In summary, here we present neurological disease correction of MPSIIIB mice by LV-mediated HSCGT, with significantly enhanced correction compared to WT HSCT. Critically LV-mediated HSCGT is relevant and scalable to MPSIIIB patients. Thus given the current lack of effective treatment for MPSIIIB, this study demonstrates that HSCGT alone or in combination with anti-inflammatories could be a clinically viable approach to improve the neurological function in MPSIIIB patients.

Acknowledgements

The authors thank the staff of the Manchester BSU for assistance. The Bioimaging Facility microscopes used in this study were purchased with grants from BBSRC, Wellcome and the University of Manchester Strategic Fund. The Histology Facility equipment used in this study was purchased by the University of Manchester Strategic Fund. Special thanks to Roger Meadows and Peter Walker for their help with microscopy and histology respectively.

Funding

This work was funded by a project grant from Action Medical Research GN2183.

References

Bigger BW, Wynn RF. Novel approaches and mechanisms in hematopoietic stem cell gene therapy. Discov Med 2014; 17(94): 207-15.

Cerbai F, Lana D, Nosi D, Petkova-Kirova P, Zecchi S, Brothers HM*, et al.* The neuron-astrocyte-microglia triad in normal brain ageing and in a model of neuroinflammation in the rat hippocampus. PLoS One 2012; 7(9): e45250.

Cressant A, Desmaris N, Verot L, Bréjot T, Froissart R, Vanier MT*, et al.* Improved behavior and neuropathology in the mouse model of Sanfilippo type IIIB disease after adeno-associated virus-mediated gene transfer in the striatum. J Neurosci 2004; 24(45): 10229-39.

Deakin JA, Lyon M. A simplified and sensitive fluorescent method for disaccharide analysis of both heparan sulfate and chondroitin/dermatan sulfates from biological samples. Glycobiology 2008; 18(6): 483-91.

DiRosario J, Divers E, Wang C, Etter J, Charrier A, Jukkola P*, et al.* Innate and adaptive immune activation in the brain of MPS IIIB mouse model. Journal of neuroscience research 2009; 87(4): 978-90.

Felger JC, Lotrich FE. Inflammatory cytokines in depression: neurobiological mechanisms and therapeutic implications. Neuroscience 2013; 246: 199-229.

Fu H, DiRosario J, Kang L, Muenzer J, McCarty DM. Restoration of central nervous system alpha-N-acetylglucosaminidase activity and therapeutic benefits in mucopolysaccharidosis IIIB mice by a single intracisternal recombinant adeno-associated viral type 2 vector delivery. J Gene Med 2010; 12(7): 624-33.

Fu H, Dirosario J, Killedar S, Zaraspe K, McCarty DM. Correction of neurological disease of mucopolysaccharidosis IIIB in adult mice by rAAV9 trans-blood-brain barrier gene delivery. Mol Ther 2011; 19(6): 1025-33.

Fu H, Kang L, Jennings JS, Moy SS, Perez A, Dirosario J*, et al.* Significantly increased lifespan and improved behavioral performances by rAAV gene delivery in adult mucopolysaccharidosis IIIB mice. Gene Ther 2007; 14(14): 1065-77.

Fu H, Meadows AS, Ware T, Mohney RP, McCarty DM. Near-Complete Correction of Profound Metabolomic Impairments Corresponding to Functional Benefit in MPS IIIB Mice after IV rAAV9-hNAGLU Gene Delivery. Mol Ther 2017; 25(3): 792-802.

Fu H, Samulski RJ, McCown TJ, Picornell YJ, Fletcher D, Muenzer J. Neurological correction of lysosomal storage in a mucopolysaccharidosis IIIB mouse model by adeno-associated virus-mediated gene delivery. Mol Ther 2002; 5(1): 42-9.

Gografe SI, Sanberg PR, Chamizo W, Monforte H, Garbuzova-Davis S. Novel pathologic findings associated with urinary retention in a mouse model of mucopolysaccharidosis type IIIB. Comp Med 2009; 59(2): 139-46.

Hareendran S, Balakrishnan B, Sen D, Kumar S, Srivastava A, Jayandharan GR. Adeno-associated virus (AAV) vectors in gene therapy: immune challenges and strategies to circumvent them. Rev Med Virol 2013; 23(6): 399-413.

Heldermon CD, Ohlemiller KK, Herzog ED, Vogler C, Qin E, Wozniak DF*, et al.* Therapeutic efficacy of bone marrow transplant, intracranial AAV-mediated gene therapy, or both in the mouse model of MPS IIIB. Mol Ther 2010; 18(5): 873-80.

Heldermon CD, Qin EY, Ohlemiller KK, Herzog ED, Brown JR, Vogler C*, et al.* Disease correction by combined neonatal intracranial AAV and systemic lentiviral gene therapy in Sanfilippo Syndrome type B mice. Gene Ther 2013; 20(9): 913-21.

Holley RJ, Deligny A, Wei W, Watson HA, Ninonuevo MR, Dagalv A*, et al.* Mucopolysaccharidosis type I, unique structure of accumulated heparan sulfate and increased N-sulfotransferase activity in mice lacking alpha-l-iduronidase. J Biol Chem 2011; 286(43): 37515-24.

Jeyakumar M, Thomas R, Elliot-Smith E, Smith DA, van der Spoel AC, d'Azzo A*, et al.* Central nervous system inflammation is a hallmark of pathogenesis in mouse models of GM1 and GM2 gangliosidosis. Brain 2003; 126(Pt 4): 974-87.

Jones SA, Breen C, Heap F, Rust S, de Ruijter J, Tump E*, et al.* A phase 1/2 study of intrathecal heparan-N-sulfatase in patients with mucopolysaccharidosis IIIA. Mol Genet Metab 2016; 118(3): 198-205.

Kan SH, Aoyagi-Scharber M, Le SQ, Vincelette J, Ohmi K, Bullens S*, et al.* Delivery of an enzyme-IGFII fusion protein to the mouse brain is therapeutic for mucopolysaccharidosis type IIIB. Proceedings of the National Academy of Sciences of the United States of America 2014a; 111(41): 14870-5.

Kan SH, Troitskaya LA, Sinow CS, Haitz K, Todd AK, Di Stefano A*, et al.* Insulin-like growth factor II peptide fusion enables uptake and lysosomal delivery of alpha-N-acetylglucosaminidase to mucopolysaccharidosis type IIIB fibroblasts. The Biochemical journal 2014b; 458(2): 281-9.

Langford-Smith A, Langford-Smith KJ, Jones SA, Wynn RF, Wraith JE, Wilkinson FL*, et al.* Female mucopolysaccharidosis IIIA mice exhibit hyperactivity and a reduced sense of danger in the open field test. PLoS One 2011a; 6(10): e25717.

Langford-Smith A, Malinowska M, Langford-Smith KJ, Wegrzyn G, Jones S, Wynn R*, et al.* Hyperactive behaviour in the mouse model of mucopolysaccharidosis IIIB in the open field and home cage environments. Genes, brain, and behavior 2011b; 10(6): 673-82.

Langford-Smith A, Wilkinson FL, Langford-Smith KJ, Holley RJ, Sergijenko A, Howe SJ*, et al.* Hematopoietic stem cell and gene therapy corrects primary neuropathology and behavior in mucopolysaccharidosis IIIA mice. Mol Ther 2012; 20(8): 1610-21.

Macauley SL, Wong AM, Shyng C, Augner DP, Dearborn JT, Pearse Y*, et al.* An anti-neuroinflammatory that targets dysregulated glia enhances the efficacy of CNS-directed gene therapy in murine infantile neuronal ceroid lipofuscinosis. J Neurosci 2014; 34(39): 13077-82.

Malinowska M, Wilkinson FL, Langford-Smith KJ, Langford-Smith A, Brown JR, Crawford BE*, et al.* Genistein improves neuropathology and corrects behaviour in a mouse model of neurodegenerative metabolic disease. PloS one 2010; 5(12): e14192.

Muenzer J, Hendriksz CJ, Fan Z, Vijayaraghavan S, Perry V, Santra S*, et al.* A phase I/II study of intrathecal idursulfase-IT in children with severe mucopolysaccharidosis II. Genet Med 2016; 18(1): 73-81.

Prasad VK, Mendizabal A, Parikh SH, Szabolcs P, Driscoll TA, Page K*, et al.* Unrelated donor umbilical cord blood transplantation for inherited metabolic disorders in 159 pediatric patients from a single center: influence of cellular composition of the graft on transplantation outcomes. Blood 2008; 112(7): 2979-89.

Reale M, Kamal MA, Velluto L, Gambi D, Di Nicola M, Greig NH. Relationship between inflammatory mediators, Aβ levels and ApoE genotype in Alzheimer disease. Curr Alzheimer Res 2012; 9(4): 447-57.

Ribera A, Haurigot V, Garcia M, Marcó S, Motas S, Villacampa P*, et al.* Biochemical, histological and functional correction of mucopolysaccharidosis type IIIB by intra-cerebrospinal fluid gene therapy. Hum Mol Genet 2015; 24(7): 2078-95.

Sardiello M, Palmieri M, di Ronza A, Medina DL, Valenza M, Gennarino VA*, et al.* A gene network regulating lysosomal biogenesis and function. Science 2009; 325(5939): 473-7.

Sergijenko A, Langford-Smith A, Liao AY, Pickford CE, McDermott J, Nowinski G*, et al.* Myeloid/Microglial driven autologous hematopoietic stem cell gene therapy corrects a neuronopathic lysosomal disease. Mol Ther 2013; 21(10): 1938-49.

Shapiro EG, Lockman LA, Balthazor M, Krivit W. Neuropsychological outcomes of several storage diseases with and without bone marrow transplantation. J Inherit Metab Dis 1995; 18(4): 413-29.

Tardieu M, Zerah M, Husson B, de Bournonville S, Deiva K, Adamsbaum C*, et al.* Intracerebral administration of adeno-associated viral vector serotype rh.10 carrying human SGSH and SUMF1 cDNAs in children with mucopolysaccharidosis type IIIA disease: results of a phase I/II trial. Hum Gene Ther 2014; 25(6): 506-16.

Tardieu M, Zérah M, Gougeon ML, Ausseil J, de Bournonville S, Husson B*, et al.* Intracerebral gene therapy in children with mucopolysaccharidosis type IIIB syndrome: an uncontrolled phase 1/2 clinical trial. Lancet Neurol 2017.

Vellodi A, Young E, New M, Pot-Mees C, Hugh-Jones K. Bone marrow transplantation for Sanfilippo disease type B. J Inherit Metab Dis 1992; 15(6): 911-8.

Wilkinson FL, Holley RJ, Langford-Smith KJ, Badrinath S, Liao A, Langford-Smith A*, et al.* Neuropathology in mouse models of mucopolysaccharidosis type I, IIIA and IIIB. PLoS One 2012; 7(4): e35787.

Wilkinson FL, Sergijenko A, Langford-Smith KJ, Malinowska M, Wynn RF, Bigger BW. Busulfan conditioning enhances engraftment of hematopoietic donor-derived cells in the brain compared with irradiation. Mol Ther 2013; 21(4): 868-76.

Zheng Y, Ryazantsev S, Ohmi K, Zhao HZ, Rozengurt N, Kohn DB*, et al.* Retrovirally transduced bone marrow has a therapeutic effect on brain in the mouse model of mucopolysaccharidosis IIIB. Mol Genet Metab 2004; 82(4): 286-95.

Figure Legends

Figure 1: Efficient expression of NAGLU from lentiviral vectors enhances survival following HSCGT.

A: Schematic of pCCL lentiviral vectors engineered to express either codon-optimised NAGLU or NAGLU-IGFII fusion proteins under the control of the internal CD11b promoter. B/C: Intracellular (B) or extracellular (C) NAGLU enzyme activity per LV-copy in the human CHME3 microglial cell line 48 hours after transduction at an MOI of 10. D: Groups used for *in vivo* study. Groups 1 (WT) and 2 (MPSIIIB) are untreated control animals. In group 3 myeloablated two month old MPSIIIB mice received WT HSCT using whole BM. In group 4 two month old myeloablated MPSIIIB mice were transplanted with HSC-enriched MPSIIIB BM transduced with LV.NAGLU. In group 5 myeloablated MPSIIIB mice received HSC-enriched MPSIIIB BM which had been transduced with LV.NAGLU-IGFII. Group 6 mice received prednisolone delivered in drinking water from 2 months of age. A combined therapy was delivery to group 7 whereby myeloablated MPSIIIB mice received HSC-enriched BM transduced with LV.NAGLU at 2 months of age, followed by prednisolone delivered in drinking water (PRED+LV.NAGLU). Thus groups 4, 5 and 7 (LV.NAGLU, LV.NAGLU-IGFII and PRED+LV.NAGLU) all received LV-mediated HSCGT treatments. WBC analysis and behaviour was performed on all mice at 6 months of age. 6-10 mice were harvested at 8 months (6 months post-transplant) for biochemical and histological analysis. A cohort (n=10-18) were kept for survival and sacrificed at their humane endpoint. E/F: VCN (E) and NAGLU enzyme activity (F) of HSC-enriched MPSIIIB BM used for transplants. G/H: LV-transduced HSC-enriched MPSIIIB BM cells at transplant were cultured for 12 days in methylcellulose culture, counting the resulting colony types (G). Total colony numbers per 2500 cells plated is shown in H. I: Donor chimerism in WBCs was determined using flow cytometry at 6 months post-transplant. J: Kaplan–Meier survival curve. A cohort of 10-18 mice per group were kept for long term analysis and sacrificed at their humane endpoint. In untreated MPSIIIB and PRED treated mice this was typically due to urine retention. K: Mean survival in months for each group. Significance is indicated by lines with *$P < 0.05$, **$P < 0.01$, ***$P < 0.001$ and ****$P < 0.0001$.

Figure 2: Superior NAGLU expression in all tissues including the brain is achieved with LV-mediated HSCGT compared to WT HSCT.

VCN (A, F, I, L and O), NAGLU activity (B, D, G, J, M and P) and β-Hex activity (C, E, H, K, N, Q) measured in WBCs, plasma, BM, brain, spleen and liver of mice at 8 months of age following the indicated treatment. LV.NAGLU, LV.NAGLU-IGFII and PRED+LV.NAGLU are all LV-mediated HSCGT-treated groups. Error bars represent the SEM. Significant differences were calculated using a one-way Anova, *P < 0.05, **P < 0.01, ***P < 0.001 and ****P < 0.0001. Significance to WT is shown above bars, all other comparisons are shown using a line.

Figure 3: Primary and secondary storage of HS and CS/DS is significantly reduced with LV-mediated HSCGT.

A-D: Glycosaminoglycan chains were extracted from the liver and brain of 8 month old mice following the indicated treatment and digested with heparinases I, II and III. Resultant disaccharides were AMAC-labelled and analysed by RP-HPLC. Total HS was measured and quantified to µg HS per mg of total protein in the liver (A) and brain (C). Relative percentage contribution of each HS disaccharide species in liver (B) and brain (D) was also calculated. E-G: Total CS/DS was measured following RP-HPLC of AMAC-labelled disaccharides generated following cABC treatment of isolated glycosaminoglycans from the liver (E) and brain (G). Amounts were quantified to µg CS/DS per mg of total protein. Relative percentage contribution of each CS/DS disaccharide species in liver (F) and brain (H) was measured. LV.NAGLU, LV.NAGLU-IGFII and PRED+LV.NAGLU are all LV-mediated HSCGT-treatment groups. Error bars represent the SEM. Significant differences were calculated using a two-way Anova using Tukey post-hoc test, *P < 0.05, **P < 0.01, ***P < 0.001 and ****P < 0.0001. Significance to WT is shown above bars, all other comparisons are illustrated using a line.

Figure 4: Reduction in inflammation and behavioural hyperactivity correction in MPSIIIB treated mice.

A-D: Quantification of cytokines MIP-1α (A), IL-1α (B), MCP-1 (C) and KC (D) in the brain at 8 months of age in the indicated treatment groups. E-I: Quantification of cytokines MIP-1α (E), IL-1α (F), MCP-1 (G), KC (H) and RANTES (I) in the liver of treated mice. J-L: IL-1α (J), MCP-1 (K) and KC (L) in plasma. M-P: Open field behaviour was performed for one hour at the same point of the circadian rhythm at 6 months of age (n = 14-22 female mice per group). The measures of hyperactivity were average speed (M), distance moved (N), frequency in

centre (O) and frequency immobile (P). LV.NAGLU, LV.NAGLU-IGFII and PRED+LV.NAGLU are all LV-mediated HSCGT-treatment groups. Error bars represent the SEM. Significant difference to WT is demonstrated with *P < 0.05, **P < 0.01, ***P < 0.001 and ****P < 0.0001. Other differences are indicated with a line.

Figure 5: Correction of astrocytic lysosomal swelling and astrocytosis following LV-mediated HSCGT but not following WT HSCT or PRED treatment.

A: LAMP2 (green), GFAP (red) and DAPI (nucleus, blue) staining in the cortex (covering layers IV/V/VI, -1.06 relative to bregma), striatum (0.14 relative to bregma), hippocampus (-1.70 relative to bregma) and amygdala (-1.70 relative to bregma) in control and transplant-treated mice. LV.NAGLU, LV.NAGLU-IGFII and PRED+LV.NAGLU are all LV-mediated HSCGT-treatment groups. Representative images are shown following staining of 6-10 mice per group. Scale bar = 50µm. B/C: Quantification of GFAP (B) and LAMP2 (C) staining using ImageJ. 2 cortex regions (x20, −0.46 and -1.06 relative to bregma) were processed per brain. Error bars represent the SEM. Significant difference to WT is demonstrated with *P < 0.05, **P < 0.01, ***P < 0.001 and ****P < 0.0001. Other differences are indicated with a line.

Figure 6: Neuronal LAMP2 is significantly reduced with LV-mediated HSCGT but not following WT HSCT or PRED treatment.

Representative images of LAMP2 (green), NeuN (red) and DAPI (nucleus, blue) staining in the cortex that correspond to a whole field of view covering cortical layers IV/V/VI (-1.06 relative to bregma), striatum (0.14 relative to bregma), hippocampus (-1.70 relative to bregma) and amygdala (-1.70 relative to bregma) in control and transplant mice. Representative images are shown following staining of 6-10 mice per group. LV.NAGLU, LV.NAGLU-IGFII and PRED+LV.NAGLU are all LV-mediated HSCGT-treatment groups. Scale bar = 50µm.

Figure 7: Correction of brain microgliosis and secondary storage with LV-mediated HSCGT but not with WT HSCT or PRED treatment.

A: IB4-positive microglia (brown) and nuclei (blue) in the cortex (layers II-VI, -1.06 relative to bregma), striatum (0.14 relative to bregma) and hippocampus (-1.70 relative to bregma) in control and transplant-treated mice. Representative images are shown following staining of 6-10 mice per group. Scale bar = 100µm. B/C: Cell counts of IB4-positive cells in the cortex (B)

or striatum (C). For cortical staining, cells were counted from two fields of view (x20 objective) per brain section, four sections per mouse (at bregma 0.14, -0.46, -1.06 and -1.7). Two fields of view were counted from the striatum at 0.98 and 0.14 relative to bregma. 6-10 mice were counted per group. D: GM2 ganglioside (black) staining of the cortex (layers IV-VI, -0.46 relative to bregma), amygdala (-1.70 relative to bregma) and hippocampus (-1.70 relative to bregma). Scale bar = 50μm. E/F: Cell counts of GM2-positive cells in the cortex (E) or amygdala (F). LV.NAGLU, LV.NAGLU-IGFII and PRED+LV.NAGLU are all LV-mediated HSCGT-treatment groups. Error bars represent SEM. Significant difference to WT is demonstrated with *P < 0.05, **P < 0.01, ***P < 0.001 and ****P < 0.0001. Other differences are indicated with a line.

Figure 8: PRED treatment reduces microgliosis in the liver.

IB4 staining (brown) and nucleus (blue) in the liver. Scale bar = 100 μm. Quantification of staining is shown using CaseViewer, measuring 8 fields of view (0.5 x 0.5μm) per mouse. LV.NAGLU, LV.NAGLU-IGFII and PRED+LV.NAGLU are all LV-mediated HSCGT-treatment groups. Error bars represent SEM. Significant difference to WT is demonstrated with *P < 0.05, **P < 0.01, ***P < 0.001 and ****P < 0.0001. Other differences are indicated with a line.

Supplementary Figure Legends:

Supplementary Figure 1: BM CFU numbers and type are unaffected in LV-mediated HSCGT animals.

At 8 months animals were sacrificed and the BM extracted. BM was cultured for 12 days in methylcellulose culture, counting the resulting colony types (A). Total number of colonies per 16,667 cells plated is shown (B). LV.NAGLU, LV.NAGLU-IGFII and PRED+LV.NAGLU are all LV-mediated HSCGT-treatment groups.

Supplementary Figure 2: Linear relationship between VCN and enzyme activity.

Plot of VCN against NAGLU enzyme activity in the indicated organs. The relationship between VCN and enzyme activity is shown using a linear regression with 95% confidence limits.

Supplementary Figure 3: Restoration of WT HS patterning following LV-mediated HSCGT.

A/B: Relative proportion of HS that was *N*-sulphated (NS), *N*-acetylated (NAc), 6-*O*-sulphated (6S), or 2-*O*-sulphated (2S) in liver (A) and brain (B) calculated from disaccharide composition following heparinase I/II/III digestion, AMAC labelling and RP-HPLC (Fig. 3). C/D: Relative proportion of CS/DS that was 2-*O*-sulphated (2S), 4-*O*-sulphated (4S) or 6-*O*-sulphated (6S) in liver (C) and brain (D) calculated from disaccharide composition analysis following cABC digestion, AMAC labelling and RP-HPLC (Fig. 3). LV.NAGLU, LV.NAGLU-IGFII and PRED+LV.NAGLU are all LV-mediated HSCGT-treatment groups. Error bars represent the SEM. Significant differences demonstrated with *P < 0.05, **P < 0.01, ***P < 0.001 and ****P < 0.0001.

Supplementary Figure 4: LAMP2 remains slightly elevated in the thalamus but is significantly reduced in the substantia nigra following LV-mediated HSCGT treatment.

LAMP2 (green), GFAP (red) and DAPI (nucleus, blue) staining in the thalamus and substantia nigra of control and transplant mice. Representative images are shown following staining of 6-10 mice per group. LV.NAGLU, LV.NAGLU-IGFII and PRED+LV.NAGLU are all LV-mediated HSCGT-treatment groups. Scale bar = 50μm.

Supplementary Figure 5: Correction of microgliosis and GM2 secondary storage in other brain regions by LV-mediated HSCGT.

A: Isolectin B4-positive microglia (brown) and nuclei (blue) in the thalamus, amygdala and substantia nigra in control and transplant-treated mice. Representative images are shown following staining of 6-10 mice per group. Scale bar = 100μm. B: GM2 secondary storage (black) in the zona incerta. Representative images are shown following staining of 6-10 mice per group. LV.NAGLU, LV.NAGLU-IGFII and PRED+LV.NAGLU are all LV-mediated HSCGT-treatment groups. Scale bar = 50μm.

Supplementary Table 1: AMAC correction factors.

Disaccharide	AMAC correction factor
ΔUA(2S)-GalNAc(4S, 6S)	1.38
ΔUA(2S)-GalNAc(4S)	1.35
ΔUA-GalNAc(4S, 6S)	1.50
ΔUA-GalNAc(4S)	1.43
ΔUA-GalNAc(6S)	1.35
ΔUA-GalNAc	1.40
ΔUA(2S)-GlcNS6S	1.25
ΔUA-GlcNS(6S)	1.13
ΔUA(2S)-GlcNS	1.00
ΔUA-GlcNS	1.04
ΔUA-GlcNAc(6S)	1.13
ΔUA-GlcNAc	1.08

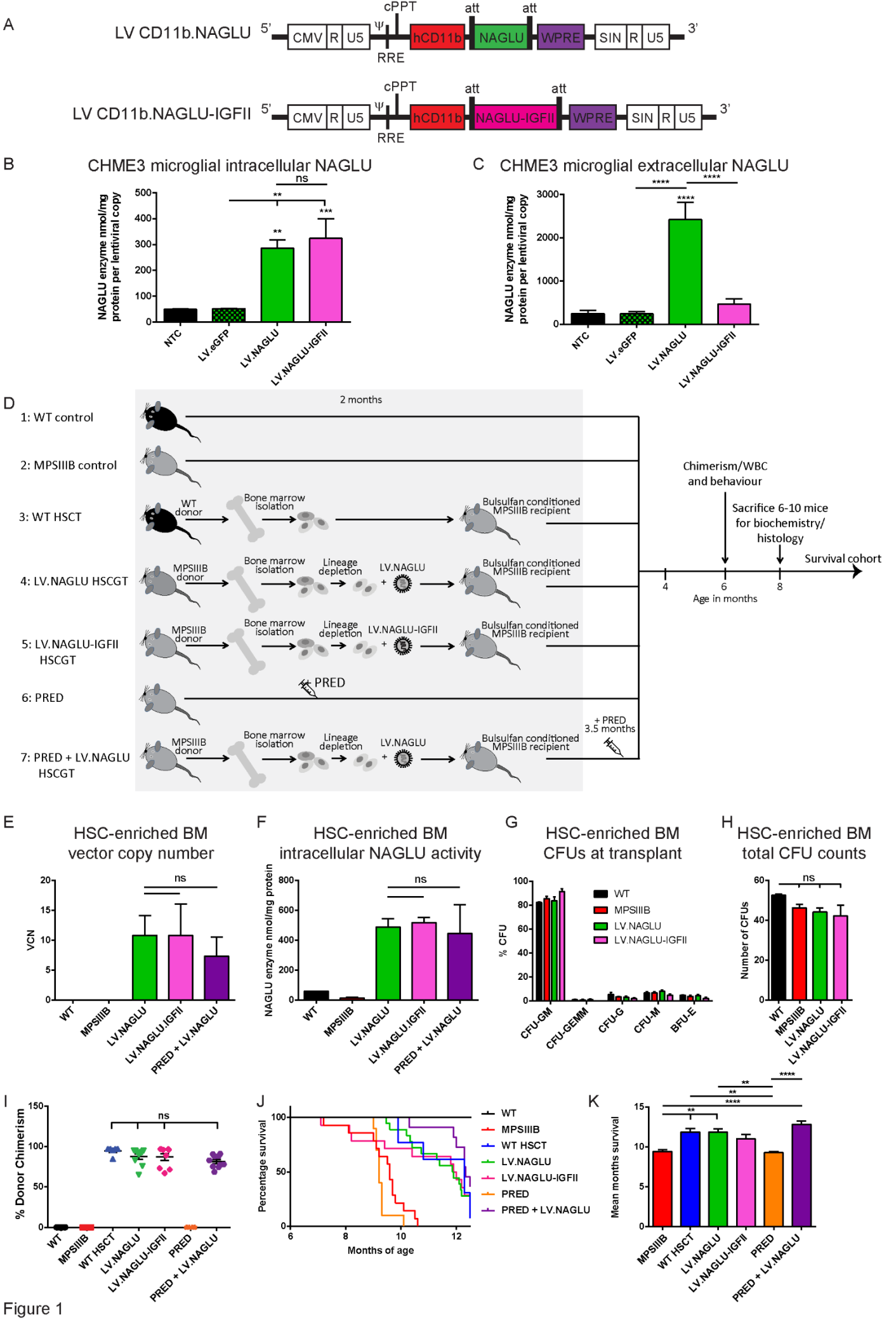
A
LV CD11b.NAGLU
5'
CMV
R
U5
Ψ
cPPT
RRE
hCD11b
att
NAGLU
att
WPRE
SIN
R
U5
3'
LV CD11b.NAGLU-IGFII
NAGLU-IGFII
B
CHME3 microglial intracellular NAGLU
NAGLU enzyme nmol/mg protein per lentiviral copy
ns
NTC
LV.eGFP
LV.NAGLU
LV.NAGLU-IGFII
C
CHME3 microglial extracellular NAGLU
D
2 months
1: WT control
2: MPSIIIB control
3: WT HSCT
WT donor
Bone marrow isolation
Bulsulfan conditioned MPSIIIB recipient
4: LV.NAGLU HSCGT
MPSIIIB donor
Lineage depletion
LV.NAGLU
5: LV.NAGLU-IGFII HSCGT
LV.NAGLU-IGFII
6: PRED
PRED
7: PRED + LV.NAGLU HSCGT
+ PRED 3.5 months
Chimerism/WBC and behaviour
Sacrifice 6-10 mice for biochemistry/ histology
Survival cohort
Age in months
E
HSC-enriched BM vector copy number
VCN
PRED + LV.NAGLU
F
HSC-enriched BM intracellular NAGLU activity
NAGLU enzyme nmol/mg protein
G
HSC-enriched BM CFUs at transplant
% CFU
CFU-GM
CFU-GEMM
CFU-G
CFU-M
BFU-E
H
HSC-enriched BM total CFU counts
Number of CFUs
I
% Donor Chimerism
WT HSCT
J
Percentage survival
Months of age
PRED + LV.NAGLU
K
Mean months survival

Figure 1

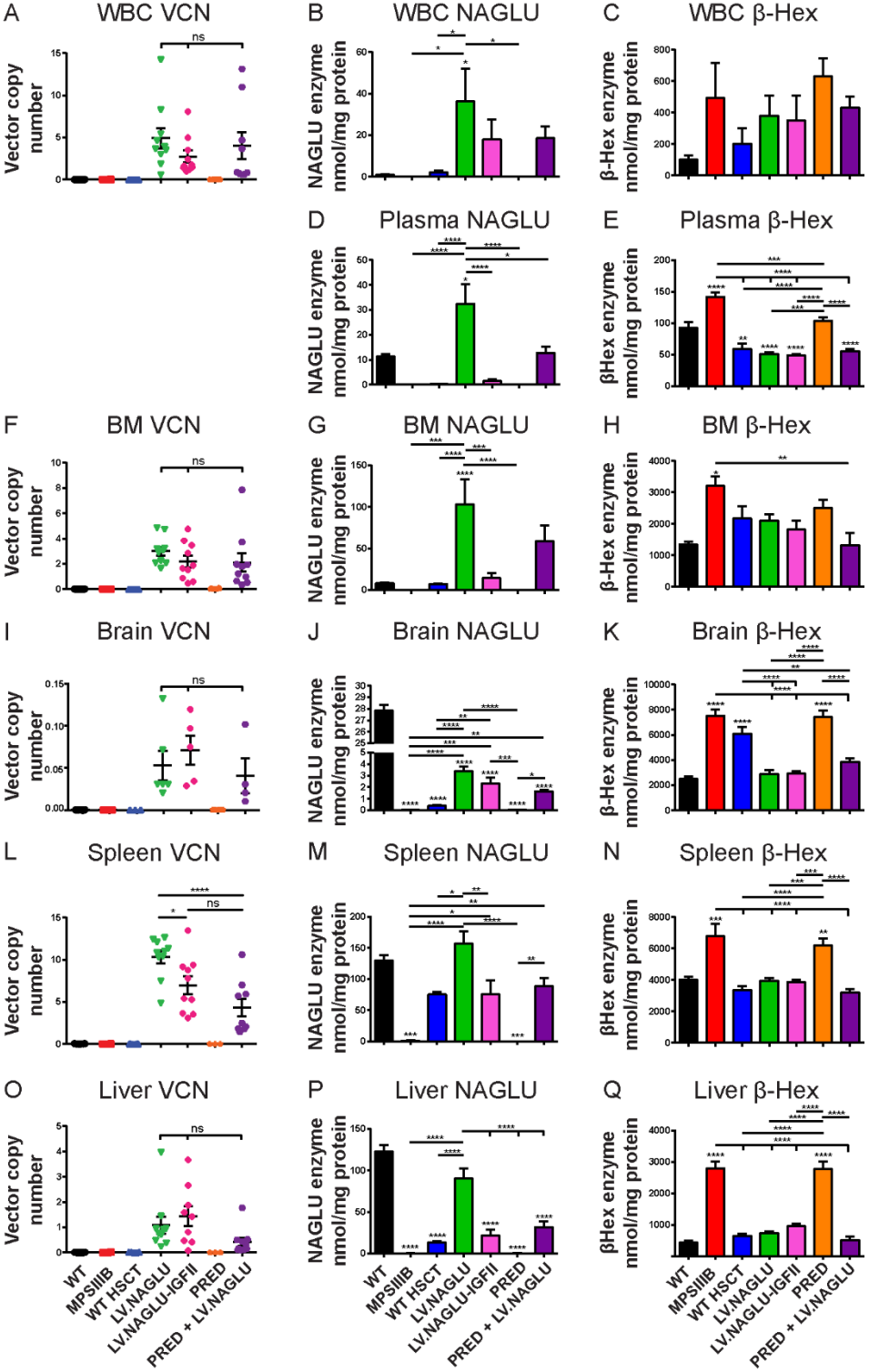
A
WBC VCN
Vector copy number
ns
B
WBC NAGLU
NAGLU enzyme nmol/mg protein
C
WBC β-Hex
β-Hex enzyme nmol/mg protein
D
Plasma NAGLU
NAGLU enzyme nmol/mg protein
E
Plasma β-Hex
βHex enzyme nmol/mg protein
F
BM VCN
Vector copy number
ns
G
BM NAGLU
NAGLU enzyme nmol/mg protein
H
BM β-Hex
β-Hex enzyme nmol/mg protein
I
Brain VCN
Vector copy number
ns
J
Brain NAGLU
NAGLU enzyme nmol/mg protein
K
Brain β-Hex
β-Hex enzyme nmol/mg protein
L
Spleen VCN
Vector copy number
ns
M
Spleen NAGLU
NAGLU enzyme nmol/mg protein
N
Spleen β-Hex
βHex enzyme nmol/mg protein
O
Liver VCN
Vector copy number
ns
P
Liver NAGLU
NAGLU enzyme nmol/mg protein
Q
Liver β-Hex
βHex enzyme nmol/mg protein
WT
MPSIIIB
WT HSCT
LV.NAGLU
LV.NAGLU-IGFII
PRED
PRED + LV.NAGLU

Figure 2

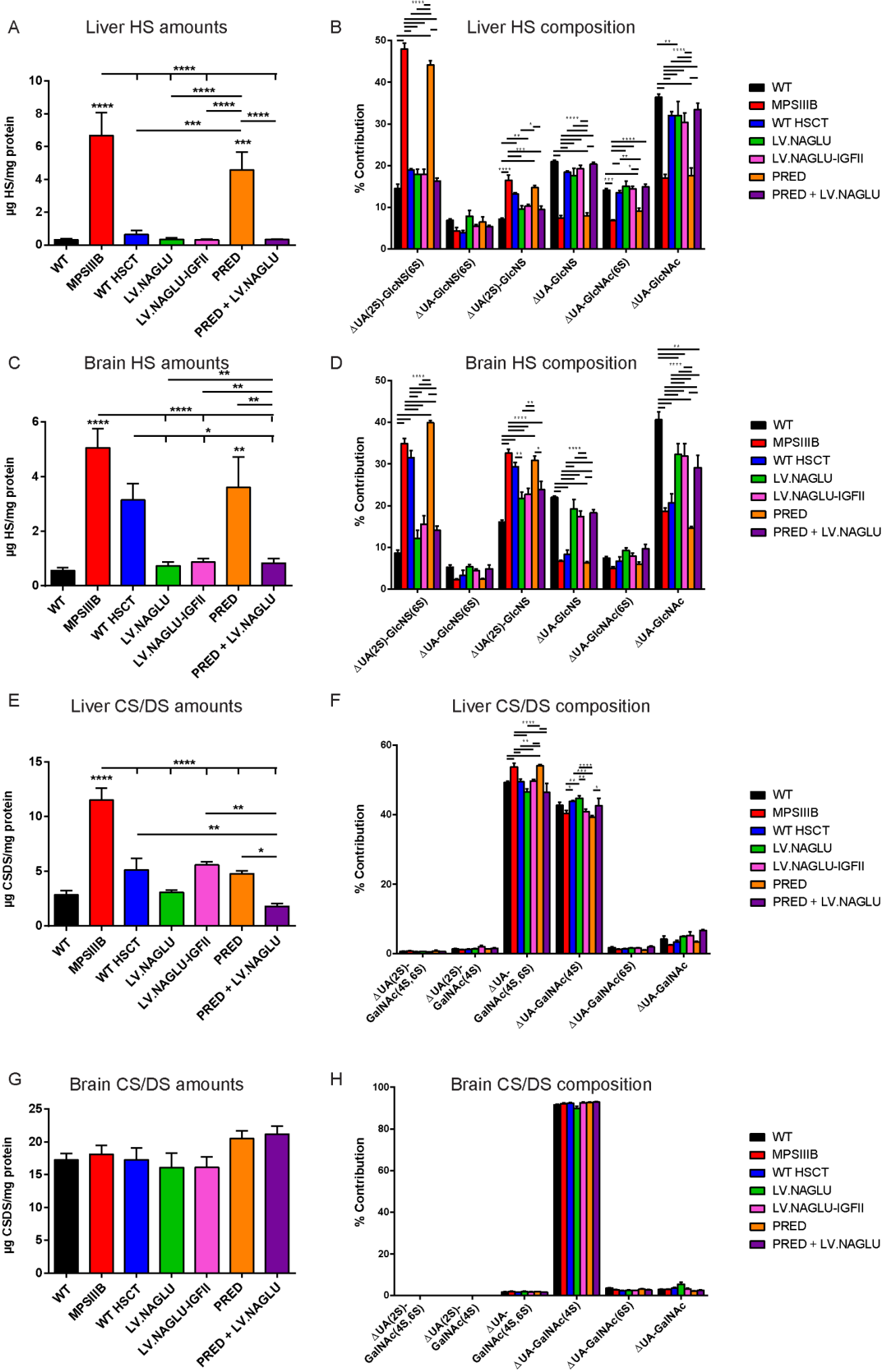
A
Liver HS amounts
µg HS/mg protein
WT
MPSIIIB
WT HSCT
LV.NAGLU
LV.NAGLU-IGFII
PRED
PRED + LV.NAGLU
B
Liver HS composition
% Contribution
ΔUA(2S)-GlcNS(6S)
ΔUA-GlcNS(6S)
ΔUA(2S)-GlcNS
ΔUA-GlcNS
ΔUA-GlcNAc(6S)
ΔUA-GlcNAc
C
Brain HS amounts
D
Brain HS composition
E
Liver CS/DS amounts
µg CSDS/mg protein
F
Liver CS/DS composition
ΔUA(2S)-GalNAc(4S,6S)
ΔUA(2S)-GalNAc(4S)
ΔUA-GalNAc(4S,6S)
ΔUA-GalNAc(4S)
ΔUA-GalNAc(6S)
ΔUA-GalNAc
G
Brain CS/DS amounts
H
Brain CS/DS composition

Figure 3

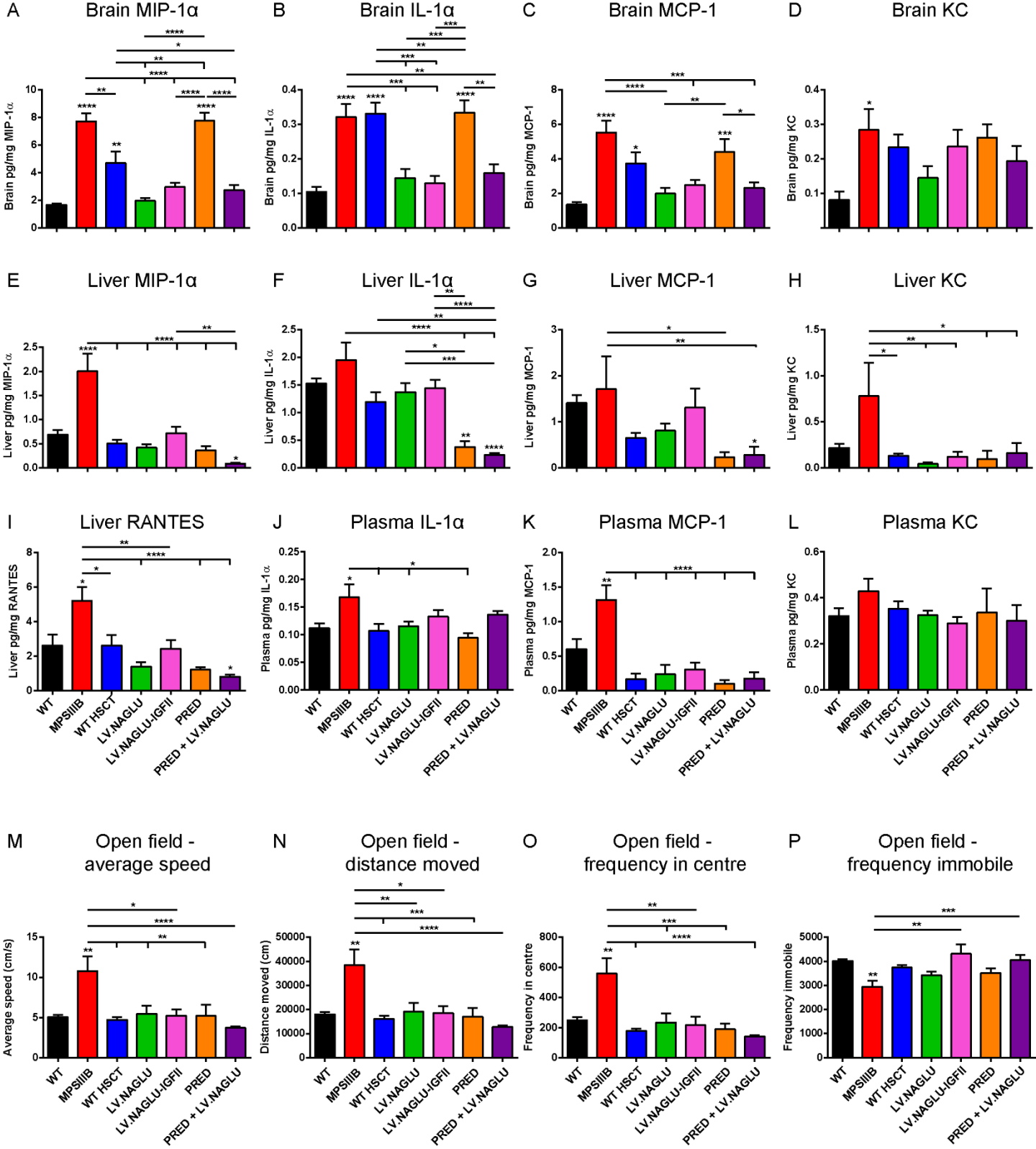
A
Brain MIP-1α
Brain pg/mg MIP-1α
B
Brain IL-1α
Brain pg/mg IL-1α
C
Brain MCP-1
Brain pg/mg MCP-1
D
Brain KC
Brain pg/mg KC
E
Liver MIP-1α
Liver pg/mg MIP-1α
F
Liver IL-1α
Liver pg/mg IL-1α
G
Liver MCP-1
Liver pg/mg MCP-1
H
Liver KC
Liver pg/mg KC
I
Liver RANTES
Liver pg/mg RANTES
J
Plasma IL-1α
Plasma pg/mg IL-1α
K
Plasma MCP-1
Plasma pg/mg MCP-1
L
Plasma KC
Plasma pg/mg KC
WT
MPSIIIB
WT HSCT
LV.NAGLU
LV.NAGLU-IGFII
PRED
PRED + LV.NAGLU
M
Open field - average speed
Average speed (cm/s)
N
Open field - distance moved
Distance moved (cm)
O
Open field - frequency in centre
Frequency in centre
P
Open field - frequency immobile
Frequency immobile

Figure 4

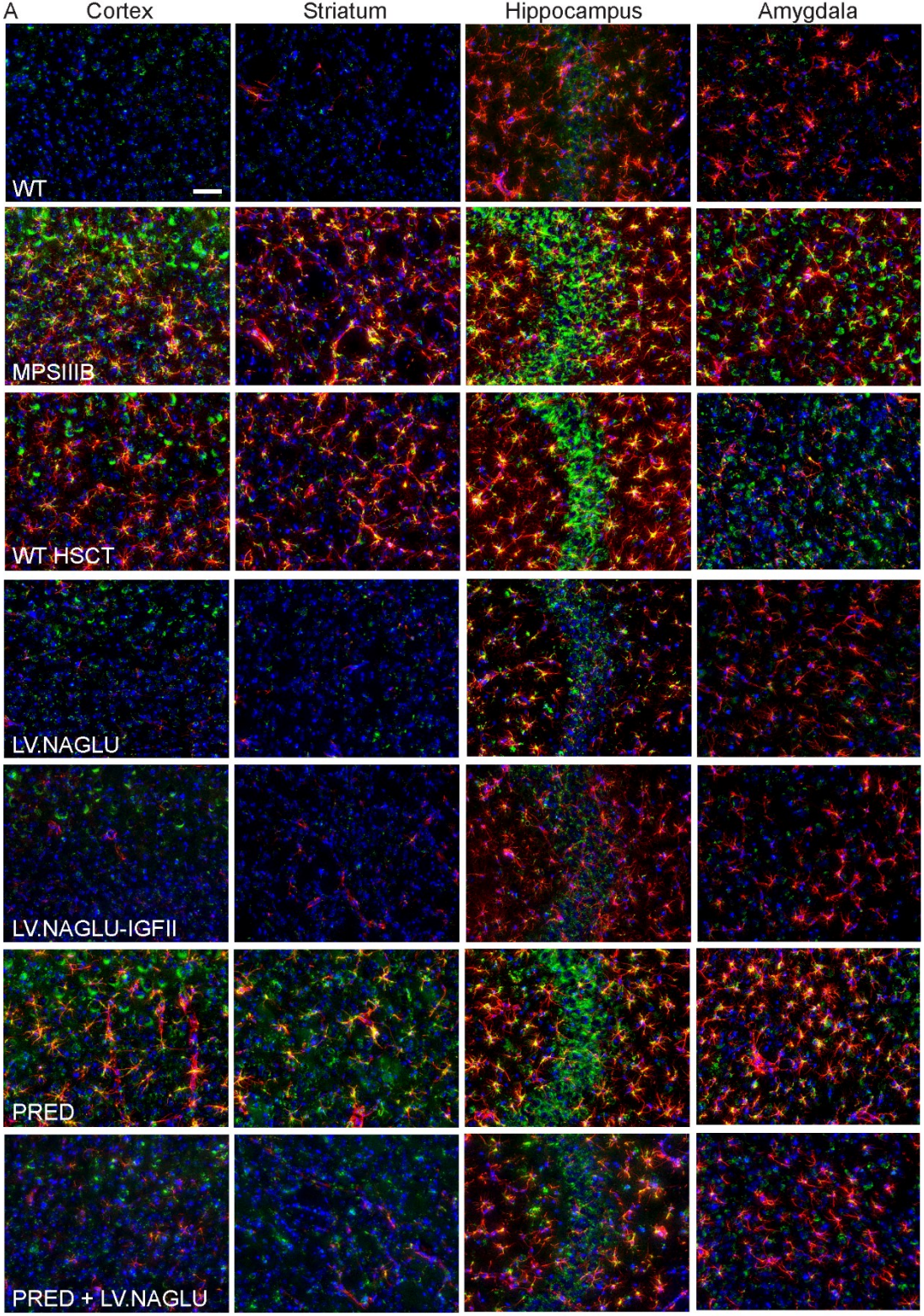
A
Cortex
Striatum
Hippocampus
Amygdala
WT
MPSIIIB
WT HSCT
LV.NAGLU
LV.NAGLU-IGFII
PRED
PRED + LV.NAGLU

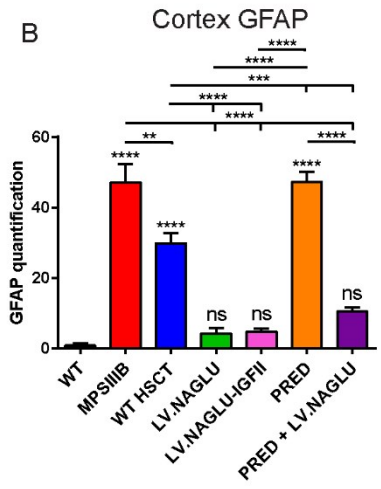
B
Cortex GFAP
GFAP quantification
WT
MPSIIIB
WT HSCT
LV.NAGLU
LV.NAGLU-IGFII
PRED
PRED + LV.NAGLU

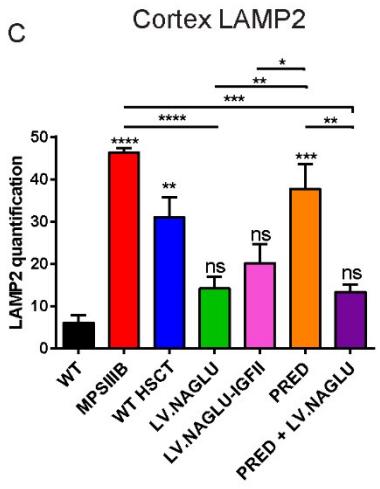
C
Cortex LAMP2
LAMP2 quantification
WT
MPSIIIB
WT HSCT
LV.NAGLU
LV.NAGLU-IGFII
PRED
PRED + LV.NAGLU

Figure 5

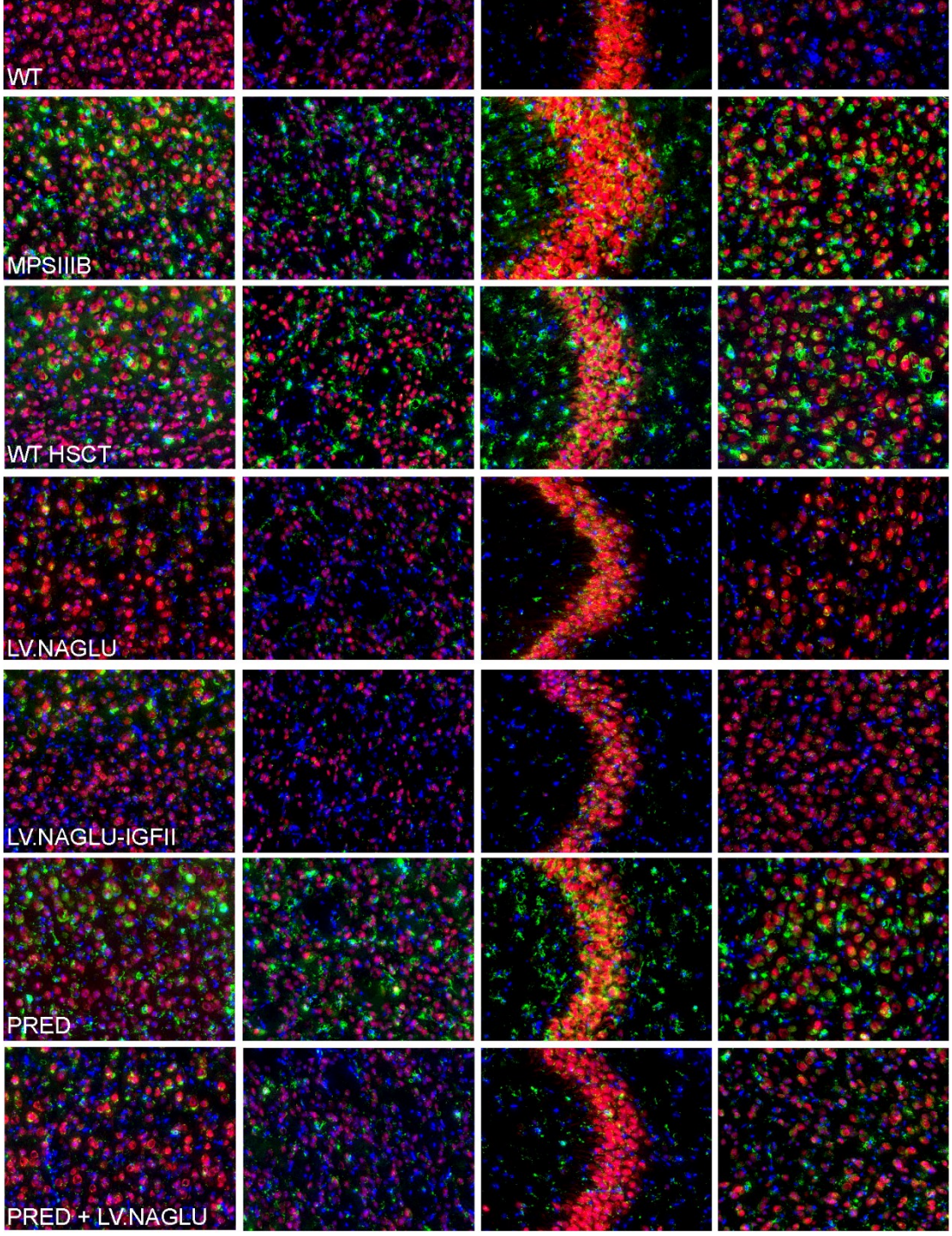

Figure 6

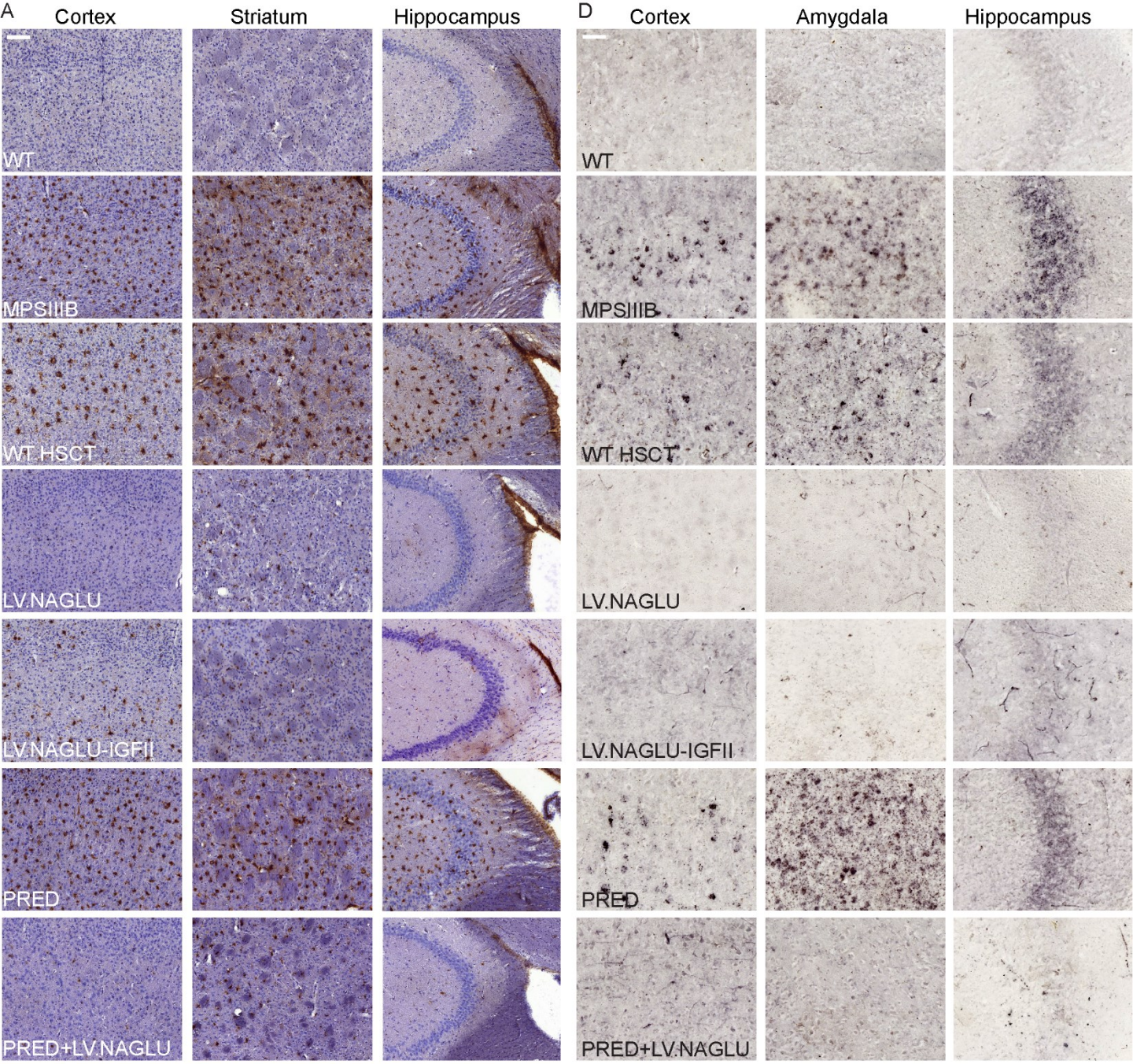
A
Cortex
Striatum
Hippocampus
WT
MPSIIIB
WT HSCT
LV.NAGLU
LV.NAGLU-IGFII
PRED
PRED+LV.NAGLU
D
Cortex
Amygdala
Hippocampus
WT
MPSIIIB
WT HSCT
LV.NAGLU
LV.NAGLU-IGFII
PRED
PRED+LV.NAGLU

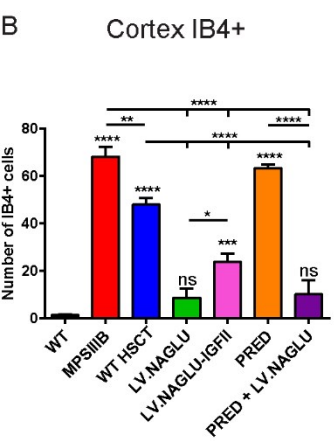
B
Cortex IB4+
Number of IB4+ cells
WT
MPSIIIB
WT HSCT
LV.NAGLU
LV.NAGLU-IGFII
PRED
PRED + LV.NAGLU

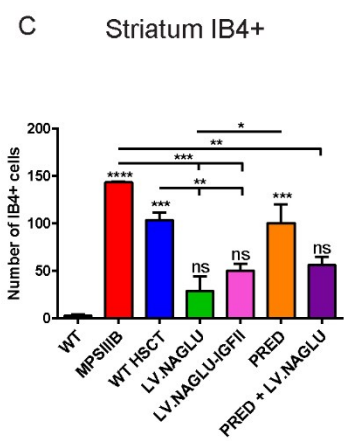
C
Striatum IB4+
Number of IB4+ cells
WT
MPSIIIB
WT HSCT
LV.NAGLU
LV.NAGLU-IGFII
PRED
PRED + LV.NAGLU

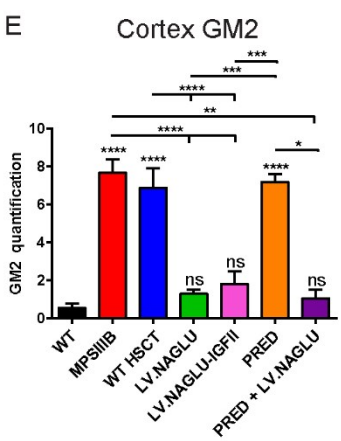
E
Cortex GM2
GM2 quantification
WT
MPSIIIB
WT HSCT
LV.NAGLU
LV.NAGLU-IGFII
PRED
PRED + LV.NAGLU

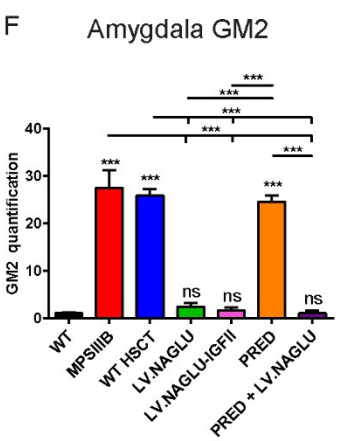
F
Amygdala GM2
GM2 quantification
WT
MPSIIIB
WT HSCT
LV.NAGLU
LV.NAGLU-IGFII
PRED
PRED + LV.NAGLU

Figure 7

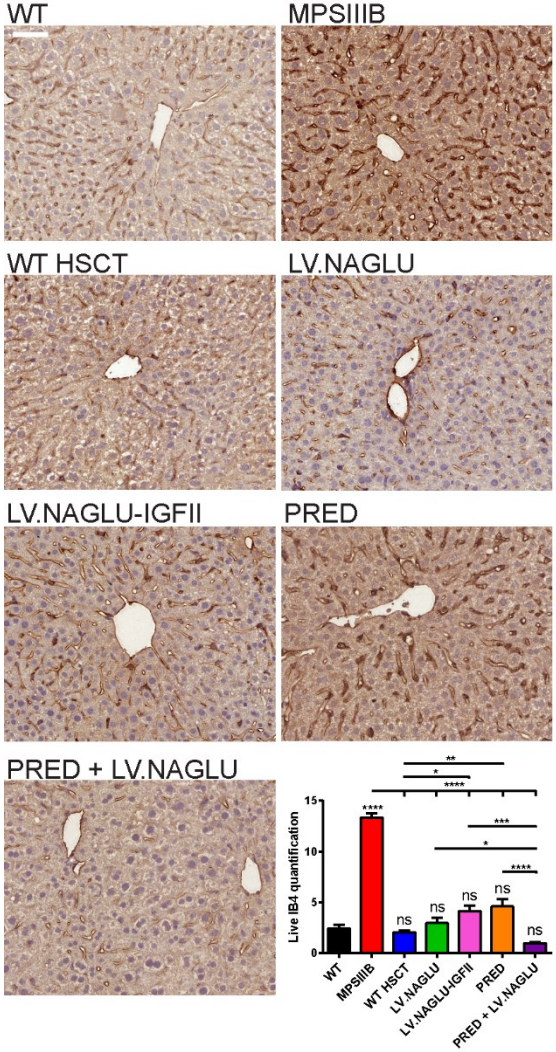
WT
MPSIIIB
WT HSCT
LV.NAGLU
LV.NAGLU-IGFII
PRED
PRED + LV.NAGLU
Live IB4 quantification
15
10
5
0
**
*
****
***
*
****
****
ns
ns
ns
ns
WT
MPSIIIB
WT HSCT
LV.NAGLU
LV.NAGLU-IGFII
PRED
PRED + LV.NAGLU

Figure 8

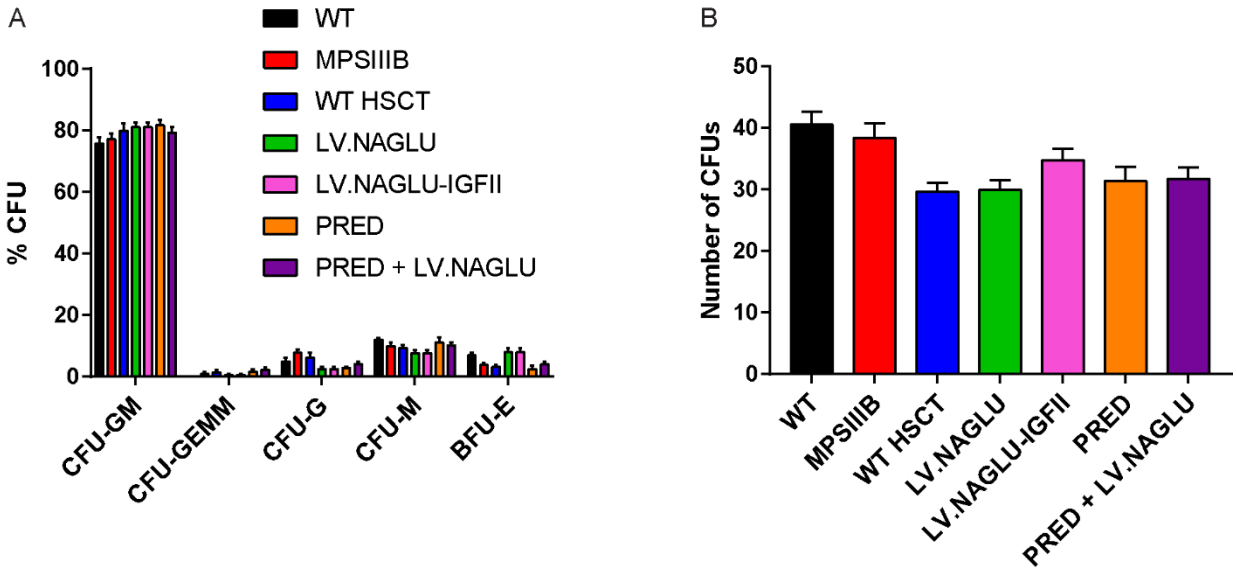

Supplementary Figure 1 - BM CFU numbers and type are unaffected in LV-mediated HSCGT animals.

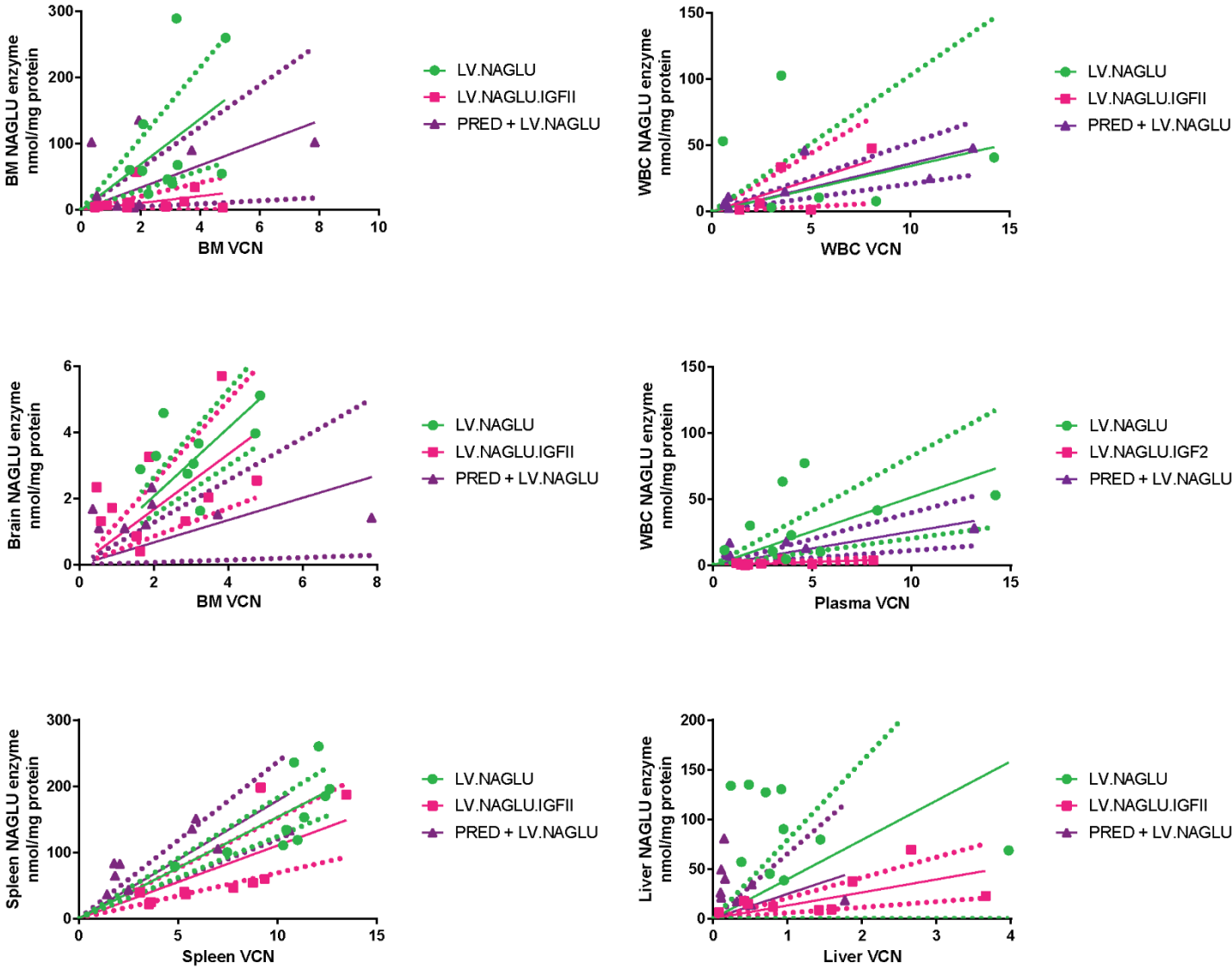

Supplementary Figure 2 - Linear relationship between VCN and enzyme activity.

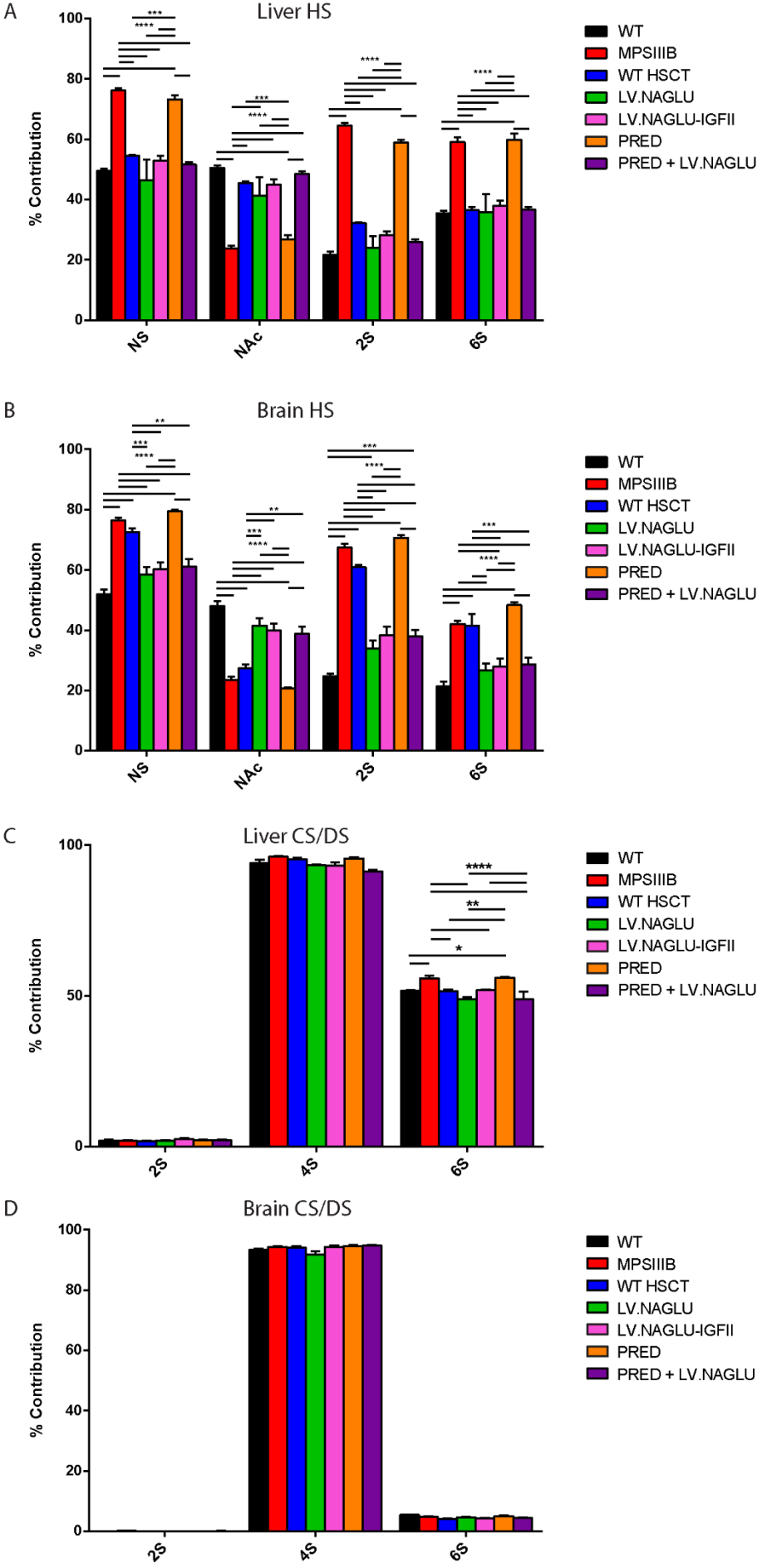

Supplementary Figure 3 - Restoration of WT HS patterning following LV-mediated HSCGT.

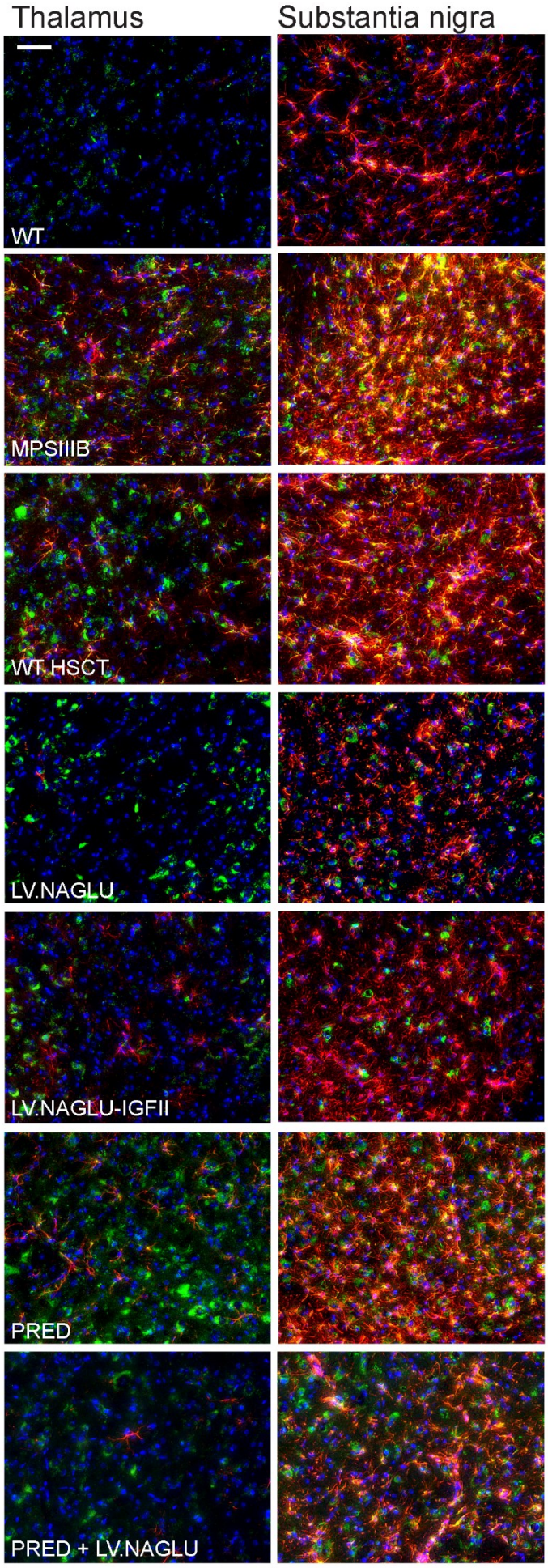

Supplementary Figure 4 - LAMP2 remains slightly elevated in the thalamus but is significantly reduced in the substantia nigra following LV-mediated HSCGT treatment.

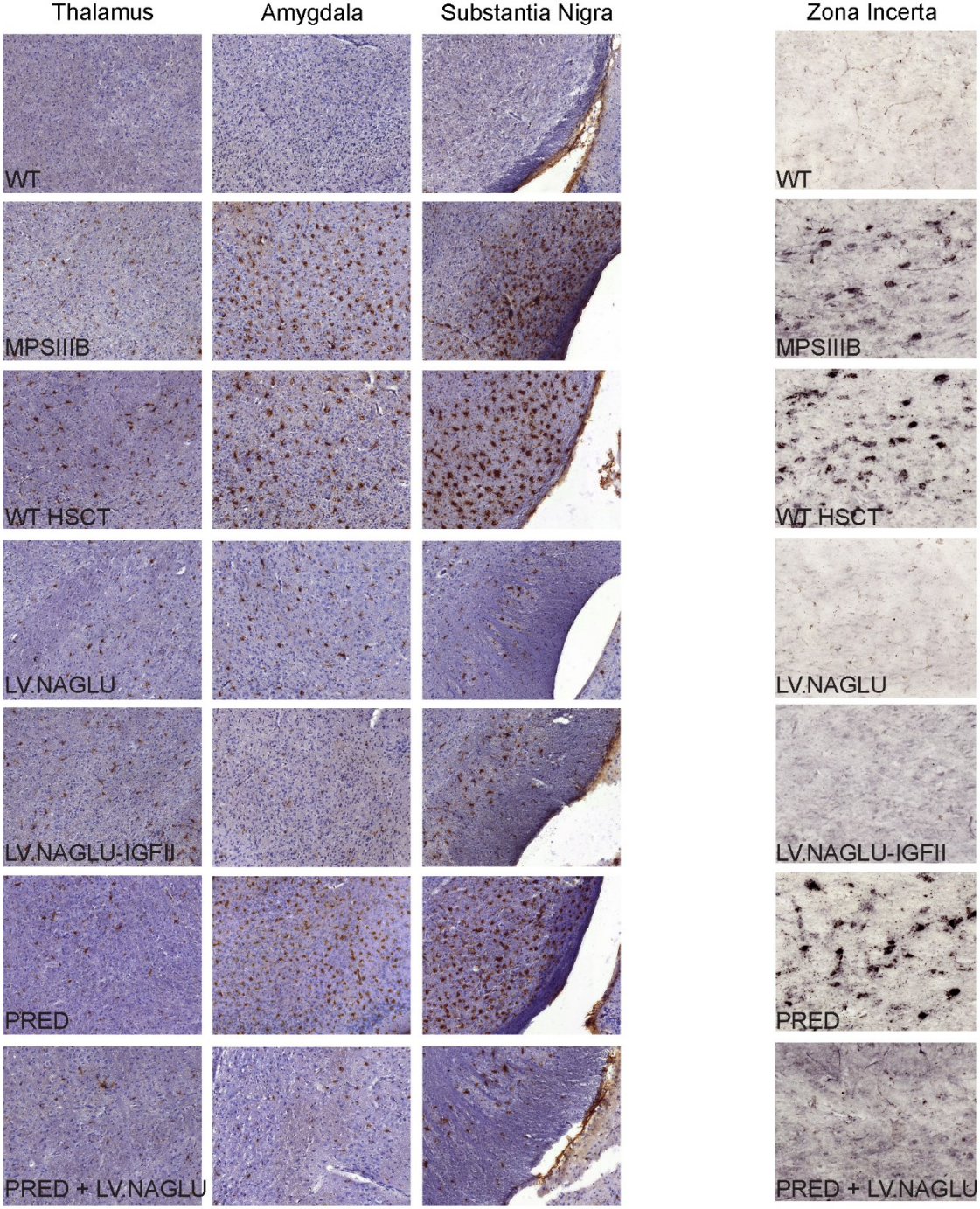

Supplementary Figure 5 - Correction of microgliosis and GM2 secondary storage in other brain regions by LV-mediated HSCGT.